



*Deep Space Network*

# 214 Pseudo-Noise and Regenerative Ranging

---

Document Owner:

Approved by:

Signature Provided 06/20/2019

Signature Provided 06/13/2019

---

Andrew O'Dea  
Telemetry, Tracking, and Command  
System Engineer Date

---

Timothy Pham  
Communications Systems Chief  
Engineer Date

Prepared By:

Released by:

Signature Provided 06/13/2019

Signature Provided 06/20/2019

---

Peter Kinman  
Telecommunications Technical  
Consultant Date

---

Christine Chang  
DSN Document Release Authority Date

---

DSN No. **810-005, 214, Rev. B**  
Issue Date: July 17, 2019  
JPL D-19379; CL# 19-4105

**Jet Propulsion Laboratory**  
California Institute of Technology

*Users must ensure that they are using the current version in DSN Telecommunications Link Design Handbook website:  
<https://deepspace.jpl.nasa.gov/dsndocs/810-005/>*

© <2019> California Institute of Technology.  
U.S. Government sponsorship acknowledged.

## Review Acknowledgment

*By signing below, the signatories acknowledge that they have reviewed this document and provided comments, if any, to the signatories on the Cover Page.*

Signature Provided

06/13/2019

Signature Provided

06/18/2019

---

Jeff Berner  
DSN Project Chief Engineer

Date

---

Scott Bryant  
DSN Ranging Cognizant Development  
Engineer

Date

***Document Change Log***

<b>Rev</b>	<b>Issue Date</b>	<b>Prepared By</b>	<b>Affected Sections or pages</b>	<b>Change Summary</b>
Initial	10/7/2003	P. W. Kinman	All	New Module
A	10/28/2015	P. W. Kinman	All	Added CCSDS range codes. Added curve fits for probability of acquisition. Added model for turn-around ranging channel with SDST AGC. Added performance comparison of PN and sequential ranging.
B	07/17/2019	P. W. Kinman	Many	Rewrote "Allocation of Link Power" section, including new models for downlink phase deviation for each of two types of turn-around ranging channels. Added new equation for chip rate. Added new information on DSS delay. Added glossary. Rewrote many paragraphs for improved clarity.

## *Contents*

<b><u>Section</u></b>	<b><u>Page</u></b>
1. Introduction.....	6
1.1 Purpose.....	6
1.2 Scope.....	6
2. General Information.....	6
2.1 System Description.....	7
2.2 Parameters Specified for Ranging Operations.....	9
2.2.1 Chip Rate and Range-Clock Frequency.....	9
2.2.2 Ranging Signal Structure.....	10
2.2.3 Integration Time.....	15
2.2.4 Uplink Ranging Modulation Index.....	16
2.2.5 Tolerance.....	16
2.3 Allocation of Link Power.....	16
2.3.1 Uplink.....	19
2.3.2 Downlink.....	20
2.4 Uplink Spectrum.....	27
2.5 Range Measurement Performance.....	29
2.5.1 Cross-Correlation Factors.....	29
2.5.2 Range Measurement Error Due to Thermal Noise.....	31
2.5.3 Probability of Acquisition.....	34
2.5.4 Processing a Set of Range Measurements.....	38
2.5.5 Comparison of PN Ranging and Sequential Ranging.....	39
2.5.6 Non-Coherent Operation.....	40
2.6 Range Corrections.....	41
2.6.1 DSS Delay.....	42
2.6.2 Z-Correction.....	43
2.7 Total Error for Range Measurement.....	44
Appendix: Glossary of Parameters.....	45
References.....	47

## *Illustrations*

<b><u>Figure</u></b>	<b><u>Page</u></b>
Figure 1. The DSN Ranging System Architecture.....	8
Figure 2. PN Ranging Signal When Third Harmonic of Range Clock is Blocked.....	15
Figure 3. Bessel Functions of the First Kind of Order 0 and 1 .....	20
Figure 4. Downlink rms Phase Deviation by Ranging Signal (No Command Feedthrough).....	23
Figure 5. Downlink rms Phase Deviation by Noise (No Command Feedthrough) .....	24
Figure 6. Downlink Ranging-Signal Power to Total Power (No Telemetry, No Command) .....	26
Figure 7. Downlink Carrier Suppression (No Telemetry, No Command).....	26
Figure 8. Uplink Spectrum for the DSN Range Code Ranging Signal.....	29
Figure 9. Standard Deviation of Range Measurement Error for the DSN and T4B Codes .....	32
Figure 10. Standard Deviation of Range Measurement Error for the T2B Code .....	33
Figure 11. Probability of Acquisition for the DSN Range Code and the T4B Code.....	37
Figure 12. Probability of Acquisition for the T2B Code .....	37
Figure 13. Comparison of Sequential Ranging and PN Ranging .....	40
Figure 14. DSS Delay Calibration .....	42
Figure 15. DSS Delay as a Function of Downlink Frequency.....	43

## *Tables*

<b><u>Table</u></b>	<b><u>Page</u></b>
Table 1. CCSDS Chip Rates .....	11
Table 2. Component Codes.....	12
Table 3. Cross-Correlation Factors, DSN Range Code .....	30
Table 4. Cross-Correlation Factors, T4B (Reference 4) .....	30
Table 5. Cross-Correlation Factors, T2B (Reference 4) .....	30
Table 6. Interpolation Table.....	36
Table 7. Parameters for Equation (62).....	38

## **1. Introduction**

### **1.1 Purpose**

This module describes capabilities of the Deep Space Network (DSN) for pseudo-noise (PN) ranging. These capabilities are available within the 70-m, the 34-m High Efficiency (HEF), and the 34-m Beam Waveguide (BWG) subnets. Performance depends on whether the spacecraft transponder uses a turn-around (non-regenerative) ranging channel or a regenerative ranging channel. Performance parameters are provided for both cases.

### **1.2 Scope**

The material contained in this module covers the PN ranging system that may be utilized by both near-Earth and deep-space missions. This document describes those parameters and operational considerations that are independent of the particular antenna being used to provide the telecommunications link. For antenna-dependent parameters, refer to Module 101, 103, or 104 of this handbook. The other ranging scheme employed by the DSN is sequential ranging, described in Module 203.

An overview of the ranging system is given in Section 2.1. The parameters to be specified for ranging operations are explained in Section 2.2. The distribution of link power is characterized in Section 2.3. The spectrum of an uplink carrier modulated by a PN ranging signal is discussed in Section 2.4. The performance of turn-around and regenerative ranging is summarized in Section 2.5. Non-coherent ranging is also discussed there. Section 2.6 describes the corrections required to determine the actual range to a spacecraft. The total error for a range measurement is discussed in Section 2.7.

## **2. General Information**

The ranging signal of interest in this module is a logical combination of a range clock and several PN codes; this signaling technique is called PN ranging. A different signaling technique, sequential ranging, is also supported by the DSN. The same instrumentation within the DSN supports both PN ranging and sequential ranging. However, there are performance differences between these two signaling techniques. This module only discusses PN ranging. Sequential ranging is discussed in Module 203.

A spacecraft transponder may have either a turn-around ranging channel or a regenerative ranging channel. The DSN processes a PN ranging signal in the same way for both types of transponder ranging channel. The performance of a PN range measurement will generally be better when the transponder uses a regenerative ranging channel. This module characterizes the performance of both regenerative ranging and non-regenerative (turn-around) ranging when the PN-ranging signaling technique is employed.

The range clock is coherently related to the carrier. The uplink carrier is often tuned during a tracking pass, in order to compensate for the Doppler effect on the uplink carrier, thereby reducing stress on the transponder's carrier-tracking loop. As the uplink carrier is tuned, the range-clock frequency varies proportionately.

In two-way ranging, one Deep Space Station (DSS) both transmits the uplink and receives the downlink. For two-way ranging, the user may calculate the round-trip light time (RTLTL) from data provided by the DSN: phase measurements of the ranging signal and a record of the transmitted uplink carrier frequency.

Three-way ranging is also supported, for which one DSS transmits the uplink and a different DSS receives the downlink. As with two-way ranging, the DSN reports phase measurements of the ranging signal and a record of the uplink-carrier frequency. From these data, the user may calculate the light time for the travel of the ranging signal from the uplink DSS, through the spacecraft, to the downlink DSS.

To put matters in perspective, the measurements discussed here are phase measurements and the resulting data permit the user to calculate time delays. Range cannot be calculated directly and accurately from the time delays because the range changes significantly over the course of the signal travel time. Similar measurement techniques employed in terrestrial applications, where the distances and measurement times are much smaller, typically permit the calculation of the range as the two-way time delay times the speed of an electromagnetic wave divided by 2. That has been the justification for using the term range measurement for this class of measurement technique. The two-way and three-way time delays calculated for deep-space missions are useful in the orbit determination process. These calculated delays assist in the improvement of trajectory models; and so, indirectly, the delays assist in the estimation of range as a function of time.

It is customary to quote range measurement error in units of meters. For two-way ranging, the range error is defined as the error in the two-way time delay times the speed of electromagnetic waves in vacuum divided by 2. (The division by two accounts for the fact that range is a one-way distance but the time delay is two-way.)

## **2.1      *System Description***

The DSN ranging system records the phase of the ranging signal that is transmitted and measures the phase of the ranging signal that returns. For two-way ranging, both recorded phase values (that of the uplink ranging signal and that of the downlink ranging signal) apply to a common instant in time, an epoch of the 1-pulse per second timing reference, which becomes the common time tag. From the difference between the uplink and downlink phases and from the history of the transmitted range-clock frequency (which can be calculated from the history of the uplink-carrier frequency), a user may compute the RTLTL (Reference 1). This two-way time delay applies to a signal arriving at the DSS at the instant specified by the time tag.

The architecture for the DSN ranging system is shown in Figure 1. The ranging signal originates in the Uplink Subsystem (UPL). The returned signal is processed in the Downlink Tracking and Telemetry Subsystem (DTT). Both the UPL and the DTT are located at the Deep Space Communications Complex (DSCC).

The signal processing in the UPL may be summarized as follows. The Uplink Signal Generator (USG) synthesizes the range clock such that it is coherently related to the uplink carrier. The range-clock frequency equals a rational factor times the uplink carrier frequency. The USG generates the ranging signal, which is the range clock modified by additional signal structure that makes possible resolution of the phase ambiguity. A sample of

the uplink phase, which is required for the delay measurement, is passed from the USG to the Uplink Processor Assembly (UPA). The USG modulates the uplink carrier with the ranging signal. The klystron supplies the final stage of power amplification for the uplink carrier.

The downlink carrier, after amplification within the Low-Noise Amplifier (LNA), passes to the DTT. Frequency down-conversion to an intermediate frequency (IF) takes place in the RF-to-IF Downconverter (RID). The IF signal is sent to an IF-to-Digital Converter (IDC). Demodulation of the IF carrier occurs in the Receiver, Ranging and Telemetry (RRT) processor. Also within the RRT, the correlation of the received, baseband ranging signal with a local model produces a measurement of the downlink phase. This downlink phase is passed to the Downlink Channel Controller (DCC).

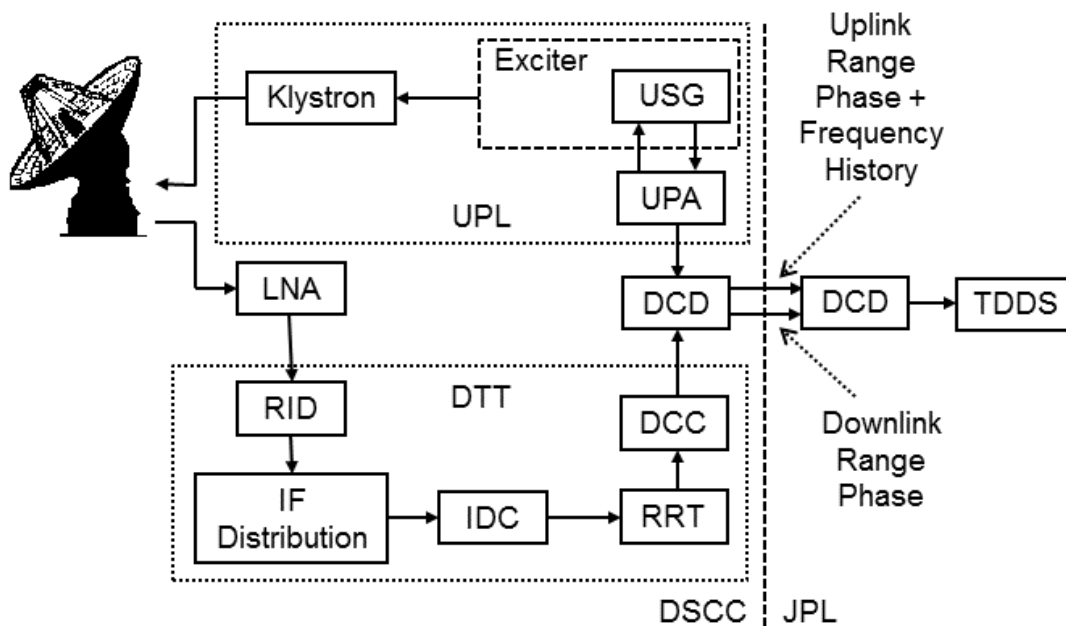


Figure 1. The DSN Ranging System Architecture

Uplink phase samples, each corresponding to an epoch of the 1-PPS (pulse per second) clock, are passed from the UPA, via the Data Capture and Delivery (DCD) software, to the Tracking Data Delivery Subsystem (TDSS), located in Pasadena. The DCC passes the downlink phase measurement and its time tag (an epoch of the 1-PPS clock), via the DCD, to the TDSS. A history of the uplink range clock's frequency is also needed for the calculation of the two-way time delay. Since the uplink range clock is coherently related to the uplink carrier, this necessary information can be derived from the history of the uplink carrier frequency, which is supplied by the UPA to the TDSS. All data required for the two-way delay calculation are archived by the TDSS for later use by a navigation team or other users.

The IDC, RRT, and DCC required for the processing of a downlink carrier are located within a Downlink Channel Processing Cabinet (DCPC). Each DCPC supports a single channel. For spacecraft with multiple channels (for example, X-band and Ka-band), or for

multiple spacecraft within a single antenna beamwidth, multiple DCPCs will be assigned to that antenna.

The DSN uses the Range Unit (RU) to deliver the difference of the ranging signal's uplink phase and downlink phase. Since the range clock and the carrier are coherently related, it is permissible to define the RU in terms of carrier phase. For an S-band uplink, the RU is defined as two cycles of the carrier. For an X-band uplink, one RU is (749/221) times two cycles of the carrier. For a Ka-band uplink, one RU is (3599/221) times two cycles of the carrier. Because the RU is defined with a factor (1 for an S-band uplink, 749/221 for an X-band uplink, and 3599/221 for a Ka-band uplink) that is proportional to frequency, the RU is proportional to time delay. (But the RU is a dimensionless unit.) One RU corresponds to approximately 0.94 ns of time delay.

A user may convert a two-way phase delay in RU into a two-way time delay as follows:

$$\text{Two-way Time Delay} = \begin{cases} \frac{2 \times RU}{f_S}, & \text{S-band uplink} \\ \frac{749}{221} \cdot \frac{2 \times RU}{f_X}, & \text{X-band uplink} \\ \frac{3599}{221} \cdot \frac{2 \times RU}{f_{Ka}}, & \text{Ka-band uplink} \end{cases} \quad (1)$$

where  $f_S$  is the frequency of an S-band uplink carrier,  $f_X$  is the frequency of an X-band uplink carrier, and  $f_{Ka}$  is the frequency of a Ka-band uplink carrier. For example, if the uplink carrier is in the X band with a frequency of 7.16 GHz and the two-way phase delay is reported as 6,500,000 RU, then the two-way time delay is 6,153,467 ns.

## 2.2 *Parameters Specified for Ranging Operations*

The following subsections present the parameters that are required in ranging operations.

### 2.2.1 *Chip Rate and Range-Clock Frequency*

In the PN ranging system, the PN ranging signal is created by filtering a composite code, where timing is defined by the range clock. The chip rate  $f_{\text{chip}}$  for the composite code is defined in terms of a rational factor  $A/B$  (a ratio of two positive integers).

$$f_{\text{chip}} = \begin{cases} \frac{A}{B} \times f_S, & \text{S-band uplink} \\ \frac{221}{749} \times \frac{A}{B} \times f_X, & \text{X-band uplink} \\ \frac{221}{3599} \times \frac{A}{B} \times f_{Ka}, & \text{Ka-band uplink} \end{cases} \quad (2)$$

$f_S$  is the frequency of an S-band uplink carrier,  $f_X$  is the frequency of an X-band uplink carrier, and  $f_{Ka}$  is the frequency of a Ka-band uplink carrier.  $A/B$  is defined, in turn, by the whole numbers  $l_{CR}$  and  $k_{CR}$  (Reference 2).

$$\frac{A}{B} = \frac{l_{CR}}{128 \cdot 2^{k_{CR}}} \quad (3)$$

The chip rate is coherently related to the uplink carrier frequency, as suggested by Equation (2).  $l_{CR}$  and  $k_{CR}$  are whole numbers that together determine the rational factor  $A/B$  relating  $f_{\text{chip}}$  to the uplink carrier frequency. Table 1 lists the selections for  $l_{CR}$  and  $k_{CR}$ . This table also indicates the approximate value of the chip rate that corresponds to each pair of whole numbers  $l_{CR}$  and  $k_{CR}$ . The exact chip rate depends, as indicated in Equation (2), on the uplink carrier frequency (and, therefore, on the channel assignment and on any Doppler compensation that may be done on the uplink).

The range clock is a periodic signal. Each half-cycle of the range clock corresponds to one chip. Therefore,

$$f_{RC} = \frac{f_{\text{chip}}}{2} \quad (4)$$

The approximate value of  $f_{RC}$  is given in Table 1 for numbers pairs  $l_{CR}$  and  $k_{CR}$  of that table. The exact value of  $f_{RC}$  depends on the uplink carrier frequency.

The DTT receiver uses the range clock in two ways. First, the phase of the range clock is measured; this determines the accuracy of the range measurement. Second, the receiver achieves chip synchronization using the range clock; this is a necessary precursor to resolving the ambiguity.

## 2.2.2 *Ranging Signal Structure*

In the PN ranging system, a filtered composite code is used for ranging. The timing of the composite code is set by the range clock. Three different composite codes are available: the DSN range code, the CCSDS T4B code, and the CCSDS T2B code. Each of these composite codes is built from a common set of component codes. The three composite codes differ from each other because of the manner in which the component codes are combined.

### 2.2.2.1 *Component Codes*

Table 2 lists the component codes. In this table, a component code is represented as a finite-length sequence of bits. The length of the  $n$ -th component code is denoted  $\lambda_n$  for  $1 \leq n \leq 6$ . The lengths are:  $\lambda_1 = 2$ ,  $\lambda_2 = 7$ ,  $\lambda_3 = 11$ ,  $\lambda_4 = 15$ ,  $\lambda_5 = 19$ , and  $\lambda_6 = 23$ . (The first component code is the 2-bit sequence representing the range clock.) The  $n$ -th component code is denoted  $b_n(i)$ , where  $i$  represents a discrete-time index,  $0 \leq i < \lambda_n$ . The proper order of each of these component codes is determined by reading the bits in each row from left to right. So, for example, the first three bits of  $b_3(\cdot)$  are all 1s and the final bit is a 0.

It is also useful to represent each component code as a sequence of chips (with the bi-polar values  $\pm 1$ ).

$$c_n(i) = 2 b_n(i) - 1 \quad (5)$$

where  $c_n(i) = \pm 1$ . Equation (5) translates a binary 1 into +1 and a logical 0 into -1.

Table 1. CCSDS Chip Rates

$l_{CR}$	$k_{CR}$	$A/B$	Approximate value of $f_{chip}$	Approximate value of $f_{RC}$
94*	6	47/4096	24 MHz	12 MHz
64	6	1/128	16 MHz	8 MHz
32	6	1/256	8 MHz	4 MHz
16	6	1/512	4 MHz	2 MHz
12	6	3/2048	3 MHz	1.5 MHz
11	6	11/8192	2.8 MHz	1.4 MHz
10	6	5/4096	2.6 MHz	1.3 MHz
9	6	9/8192	2.3 MHz	1.15 MHz
8	6	1/1024	2 MHz	1 MHz
7	6	7/8192	1.8 MHz	900 kHz
6	6	3/4096	1.5 MHz	750 kHz
5	6	5/8192	1.3 MHz	650 kHz
4	6	1/2048	1 MHz	500 kHz
3	6	3/8192	750 kHz	375 kHz
2	6	1/4096	500 kHz	250 kHz
1	6	1/8192	250 kHz	125 kHz
2	8	1/16384	128 kHz	64 kHz
2	9	1/32768	64 kHz	32 kHz
2	10	1/65536	32 kHz	16 kHz

\*This rate is used by the Bepi-Colombo mission and is outside defined CCSDS rates

Table 2. Component Codes

$b_n$	code	$\lambda_n$
$b_1$	1, 0	2
$b_2$	1, 1, 1, 0, 0, 1, 0	7
$b_3$	1, 1, 1, 0, 0, 0, 1, 0, 1, 1, 0	11
$b_4$	1, 1, 1, 1, 0, 0, 0, 1, 0, 0, 1, 1, 0, 1, 0	15
$b_5$	1, 1, 1, 1, 0, 1, 0, 1, 0, 0, 0, 0, 0, 1, 1, 0, 1, 1, 0, 0	19
$b_6$	1, 1, 1, 1, 1, 0, 1, 0, 1, 1, 0, 0, 1, 1, 0, 0, 1, 0, 1, 0, 0, 0, 0	23

### 2.2.2.2 DSN Range Code

The DSN range code (also called the JPL range code) was the first composite code to be implemented and validated with the current ranging instrumentation in the DSN. Following is an explanation of how this composite code is generated from the component codes listed in Table 2.

For each finite-length PN code  $b_n(i)$ , a periodic code  $b_n'(i)$  of period  $\lambda_n$  is formed by endless repetition:

$$b_n'(i) = b_n(i \bmod \lambda_n) \quad (6)$$

where  $b_n'(i)$  is binary valued. In this document, the prime (') indicates a periodic sequence (made from a finite-length sequence by periodic extension).

The composite code is

$$b'(i) = b_1'(i) \cup [b_2'(i) \cap b_3'(i) \cap b_4'(i) \cap b_5'(i) \cap b_6'(i)] \quad (7)$$

where  $\cup$  and  $\cap$  are the logical OR and logical AND operators, respectively. Since the component code lengths  $\lambda_n$  ( $1 \leq n \leq 6$ ) are relatively prime, the period  $L$  (in bits) of the composite code is the product of the component code lengths. That is,

$$b'(i + L) = b'(i) \quad (8)$$

where

$$L = \prod_{n=1}^6 \lambda_n = 1,009,470 \quad (9)$$

The periodic chip sequence corresponding to the periodic bit sequence  $b'(i)$  is

$$c'(i) = 2 b'(i) - 1 \quad (10)$$

where  $b'(i)$  is the periodic bit sequence of Equation (7).  $c'(i)$  is bi-polar,  $c'(i) = \pm 1$ .

In this design a large  $L$  is obtained from relatively small component code lengths. A large  $L$  is necessary for resolution of the range ambiguity, yet small  $\lambda_n$  are needed for a practical implementation of the correlators at the receiver. The ambiguity resolution of this code is given by

$$\text{ambiguity resolution} = \frac{c \cdot L}{4f_{RC}} \quad (11)$$

where  $f_{RC}$  is the range-clock frequency and  $c$  is the speed of electromagnetic waves in vacuum. For a range clock of approximately 1 MHz, the ambiguity resolution is 75,660 km.

An important property of this composite code is that it approximates a sequence of period 2 bits. The composite code equals  $b_1'(i)$ , the first component with a period of 2 bits, most of the time. The effect of the other 5 component codes is to invert a small fraction (1/32) of the logical 0s in  $b_1'(i)$ . Since  $b_1'(i)$  corresponds to the range clock, the composite code may be viewed as the range clock with an occasional inversion of a logical 0.

Most of this ranging signal's power lies at the range-clock frequency. This is desirable, since the accuracy of the range measurement is set by a correlation against a local model of the range clock. The occasional inversion is necessary to resolve the range ambiguity, but for this purpose the inversions need not be frequent.

### 2.2.2.3 *CCSDS T4B Code*

The Consultative Committee for Space Data Systems (CCSDS) recommends a composite code called T4B for use in deep-space ranging (Reference 2). The T4B code employs the same set of component codes that are used by the DSN range code (Table 2). The T4B code is constructed from the component chip sequences:

$$c_n'(i) = c_n(i \bmod \lambda_n) \quad (12)$$

where  $c_n(\cdot) = \pm 1$  is the chip sequence of length  $\lambda_n$  for the  $n$ -th component code, as given by Equation (5), and  $c_n'(\cdot)$  is its periodic extension. The periodic, composite chip sequence  $c'(i)$  is computed from the components  $c_n'(i)$  as follows:

$$c'(i) = \text{sign}[4c_1'(i) + c_2'(i) - c_3'(i) - c_4'(i) + c_5'(i) - c_6'(i)] \quad (13)$$

where  $c'(i) = \pm 1$  and where  $\text{sign}[\cdot]$  is the algebraic sign of its argument. The period of the composite code  $c'(i)$  equals  $L$ , as given in Equation (9). The ambiguity resolution of this code is the same as that for the DSN range code; this resolution is given in Equation (11).

As suggested by Equation (13), the range clock  $c_1'(i)$  has a disproportionate influence on the composite code  $c'(i)$ . The composite code may be viewed as the range clock with an occasional inversion of a chip. (With the T4B code, unlike the DSN range code, the inversion may go in either direction:  $-1 \rightarrow +1$  or  $+1 \rightarrow -1$ .) As with the DSN range code, most of the ranging signal's power lies at the range-clock frequency. As shown in Section 2.5, the performance of the T4B code is close to that of the DSN range code.

### 2.2.2.4 *CCSDS T2B Code*

The CCSDS recommends a second composite code, called T2B, which provides an alternative to the T4B code in performance trade-off space (Reference 2). The T2B code

employs the same set of component codes (Table 2) that are used by the DSN range code and the T4B code. The periodic, composite chip sequence  $c'(i)$  for the T2B code is computed from the components  $c_n'(i)$  as follows:

$$c'(i) = \text{sign}[2c_1'(i) + c_2'(i) - c_3'(i) - c_4'(i) + c_5'(i) - c_6'(i)] \quad (14)$$

The period of the T2B code equals  $L$ , as given in Equation (9). The ambiguity resolution of this code is the same as that for the T4B code and the DSN range code; this resolution is given in Equation (11).

In the construction of the T2B code, using Equation (14), the range clock  $c_1'(i)$  gets only 2 “votes”, whereas in the construction of the T4B code, using Equation (13), the range clock gets 4 “votes”. As a result, the T2B code places less power in the range clock. The T2B code will therefore generally produce a less accurate range measurement than the T4B code; however, the T2B code will achieve a better probability of acquisition for smaller received power levels.

#### 2.2.2.5 *PN Ranging Signal*

The PN ranging signal is created by filtering the composite code. This is accomplished with the uplink ranging filter, which is digitally implemented within the USG. The uplink ranging filter is a low-pass filter with a configurable bandwidth. The default (and minimum) bandwidth is 1.2 MHz. The PN ranging signal, available at the output of the uplink ranging filter, is used to phase-modulate the uplink carrier. This modulation also happens in the USG.

The purpose of the uplink ranging filter is to limit the bandwidth of the modulated uplink carrier. Because phase modulation is a non-linear modulation, the bandwidth of a carrier that is phase-modulated by the PN ranging signal can be much wider than twice the bandwidth of the PN ranging signal. If the composite code were not low-pass filtered, but instead sent directly to the phase modulator, the bandwidth of the uplink carrier would, in general, be much wider yet. (The command signal, if present, also contributes to the bandwidth of the uplink carrier, but typically the command signal has a much smaller bandwidth than the PN ranging signal. The PN ranging signal, when present, is therefore the modulating signal that plays the dominant role in determining the bandwidth of the uplink carrier.)

The bandwidth of the uplink ranging filter has a default value of 1.2 MHz. This is also the minimum bandwidth. This filter can be configured for a larger bandwidth. For a range-clock frequency larger than 1 MHz, it will be necessary to use a larger bandwidth. The decision about what bandwidth to use will be based, in part, on the effect of the filter on the PN ranging signal but also must account for spectral occupancy of the uplink carrier.

The composite code, as it appears at the input to the uplink ranging filter, is a sequence of bi-polar chips, where each chip is represented by a rectangular pulse. The uplink ranging filter will remove the highest-frequency content from this chip stream, so the PN ranging signal at the filter output will have slower transitions and smooth features. In the case where the uplink ranging filter passes the fundamental harmonic of the range clock but blocks third and higher-order harmonics of the range clock, a square-wave range clock on the filter input becomes a sinewave range clock on the filter output. The composite code on the filter input becomes on the filter output, in this case, a sequence of bi-polar chips, where each chip may be represented

approximately by a half-cycle of a sinewave. This is illustrated in Figure 2 for the first eight chips of the DSN range code. The parameter  $T_c$  is the chip period. The range-clock frequency equals  $1/(2T_c)$ . This is the desired situation for the purpose of minimizing the spectral occupancy of the uplink carrier.

The range clock is modeled, in this module, as a sinewave. The PN ranging signal is modeled as the composite code but with each chip a half-cycle of a sinewave, as depicted in Figure 2. These models are good approximations when the uplink ranging filter passes the fundamental harmonic of the range clock but blocks the third harmonic (and higher-order harmonics) of the range clock. Even if this condition is not strictly met, these models are useful as first-order approximations; they lead to performance equations that may be easily calculated. Trying to get more accurate results would typically involve computer simulations.

There is also the limiting case where the bandwidth of the uplink ranging filter is much larger than the range-clock frequency. In this limit, the range clock is a square-wave and the PN ranging signal is the composite code (with chips represented by rectangular pulses). This limiting case is only approached when the range-clock frequency is much smaller than 400 kHz (one-third of 1.2 MHz). Since the accuracy of the range measurement improves with increasing range-clock frequency, this scenario is not common.

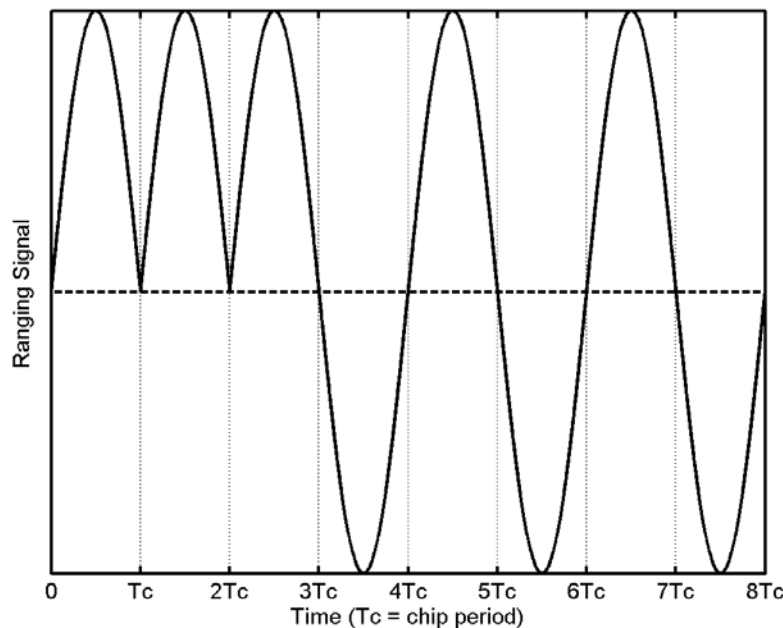


Figure 2. PN Ranging Signal When Third Harmonic of Range Clock is Blocked

### 2.2.3 *Integration Time*

The integration time  $T$  should be large enough that the probability of range measurement acquisition is close to 1.0 and the range error due to downlink thermal noise is small (see Section 2.5). In the special case of non-coherent ranging, the presence of a frequency mismatch between the received ranging signal and the local model means that there is also

reason to keep  $T$  relatively small, so that an optimum  $T$  should be carefully chosen for non-coherent ranging.

#### **2.2.4 Uplink Ranging Modulation Index**

The uplink ranging modulation index is chosen to get a suitable distribution of power among the ranging and command sidebands and the residual carrier on the uplink (see Section 2.3). With turn-around (non-regenerative) ranging, the uplink ranging modulation index also affects the distribution of power on the downlink carrier. The analysis appearing below employs an rms phase deviation of the uplink carrier. This rms phase deviation equals the peak modulation index divided by  $\sqrt{2}$  for the usual case of a sinewave range clock.

#### **2.2.5 Tolerance**

The tolerance plays a role in deciding whether to judge range acquisitions as “in lock” or “out of lock”. The ranging process does not use a phase-locked loop, so ranging lock status is estimated using the ranging probability of acquisition. For any given range acquisition, the ratio  $P_R/N_0$  of the downlink ranging signal power to the noise spectral density is measured. From this measured  $P_R/N_0$ , an estimate of the probability of acquisition  $P_{acq}$  is calculated. Section 2.5 describes the calculation of the  $P_{acq}$  from  $P_R/N_0$ .

Tolerance may be selected over the range of 0.0% to 100.0%. The default value for tolerance is 99%. An acquisition lock status depends upon the following criteria:

$P_{acq}(\%) \geq \text{Tolerance}$  results in Acquisition declared “in lock”

$P_{acq}(\%) < \text{Tolerance}$  results in Acquisition declared “out of lock”

This procedure is explained for the example where the tolerance has the default value of 99%. For a given acquisition,  $P_R/N_0$  is measured. From this measured value, the probability of acquisition  $P_{acq}$  is calculated; this number is the probability that the ambiguity is correctly resolved for this particular acquisition. Treating  $P_{acq}$  as a percentage, it is compared with the tolerance of 99%. If  $P_{acq}(\%)$  equals or exceeds 99%, the acquisition is declared “in lock”. Otherwise, it is declared “out of lock”. Note that the “out of lock” ranging data may be valid data, with a probability of  $P_{acq}(\%)$  of being correct.

### **2.3 Allocation of Link Power**

The power allocation for a link is the distribution of power among the important link components: the residual carrier, the ranging sidebands, and the data (command or telemetry) sidebands. The following notation is used here for both the uplink and downlink:

$P_C$  = power in residual carrier

$P_R$  = usable power in ranging sidebands

$P_D$  = usable power in data sidebands

$P_T$  = total link power

$P_C$  is the power in a single spectral line at the carrier frequency. When  $P_C$  is finite (greater than zero), carrier synchronization may be obtained at the receiver using a phase-locked loop that tracks this residual carrier. (Carrier synchronization may also be obtained with a Costas loop tracking the data sidebands, which are symmetrically located about the nominal carrier frequency.)

$P_R$  is that portion of the power in the ranging sidebands that is used in the range measurement.  $P_R$  includes both the spread-spectrum content arising from the PN code components as well as the two discrete spectral lines (at  $f_{RC}$  Hz above and at  $f_{RC}$  Hz below the residual carrier) that correspond to the range clock's fundamental harmonic. Higher-order harmonics (beyond the fundamental harmonic) of the range clock are not used in a range measurement and are not included in  $P_R$ . The range measurement error is determined by the discrete spectral lines of the range clock's fundamental harmonic. Ambiguity resolution is achieved using the spread-spectrum content.

For the uplink,  $P_D$  is that portion of the power in the command sidebands that is employed in command detection in the transponder. In the most common signal design for a deep-space uplink, command data modulate a sinewave subcarrier and  $P_D$  only accounts for the power in the sidebands associated with the upper and lower fundamental harmonic of the subcarrier frequency. In the case of a sinewave subcarrier, the higher-order harmonics of the subcarrier frequency are not employed in command detection in the typical transponder and are not included in  $P_D$ .

For some missions, the command signal is bi-polar. An example of this is when the command symbols, represented as rectangular pulses, directly phase-modulate the uplink carrier. In this case, the uplink  $P_D$  accounts for all power in command sidebands, since the command detection process in the typical transponder utilizes all command sidebands arising from a bi-polar command signal.

For the downlink,  $P_D$  is that portion of the power in the telemetry sidebands that is employed in telemetry detection at the station. Commonly, the telemetry signal is bi-polar; this happens when rectangular pulses (the telemetry symbols) directly phase-modulate the downlink carrier or when these symbols modulate a square-wave subcarrier that, in turn, phase-modulates the downlink carrier. In such cases, all of the power in the telemetry sidebands is employed in telemetry detection. This is a result of both the data and the subcarrier (if present) being bi-polar.

For some missions, the telemetry signal modulates a sinewave subcarrier and this composite signal phase-modulates the downlink carrier. In such a case, the downlink  $P_D$  is that portion of the power in the telemetry sidebands that is employed in telemetry detection at the station. Not included is the power in the higher-order harmonics of the subcarrier frequency.

$P_T$  is not, in general, the sum of  $P_C$ ,  $P_R$ , and  $P_D$ . In general,  $P_T$  is larger than that sum. There are multiple reasons for this. First,  $P_R$  does not account for power in the higher-order harmonics of the sinewave range clock. Second, when multiple signals (for example, a ranging signal and a telemetry signal) simultaneously phase-modulate a carrier, intermodulation products arise. These intermodulation products consume link power but do not contribute to either the range measurement or telemetry detection. Moreover, for the downlink, noise sidebands are present (in the case of turn-around ranging).

In calculating power allocations for a modulated carrier, it is necessary to characterize the level of the modulation. In this document, the root-mean-square (rms) phase deviation of the carrier will be used for this purpose. The following symbols are used in this module to represent rms phase deviation of the carrier:

uplink:	$\phi_r$	=	rms phase deviation by ranging signal, rad rms
uplink:	$\phi_{cmd}$	=	rms phase deviation by command signal, rad rms
downlink:	$\theta_{rs}$	=	rms phase deviation by ranging signal (strong signal), rad rms
downlink:	$\theta_r$	=	rms phase deviation by ranging signal, rad rms
downlink:	$\theta_{cmd}$	=	rms phase deviation by feedthrough command signal, rad rms
downlink:	$\theta_n$	=	rms phase deviation by noise, rad rms
downlink:	$\theta_{tlm}$	=	rms phase deviation by telemetry signal, rad rms

On the uplink,  $\phi_r$  and  $\phi_{cmd}$  are parameters, constant for any given tracking pass. For a sinewave range clock,  $\phi_r$  is related to the peak modulation index for uplink ranging by:

$$\phi_r = (\text{peak modulation index for uplink ranging, rad})/\sqrt{2} \quad (15)$$

When a sinewave subcarrier is used with command,  $\phi_{cmd}$  is related to the peak modulation index for command by:

$$\phi_{cmd} = (\text{peak modulation index for command, rad})/\sqrt{2}, \quad \begin{array}{l} \text{sinewave} \\ \text{subcarrier} \end{array} \quad (16)$$

However, for a bi-polar command signal,  $\phi_{cmd}$  equals the peak modulation index for command.

On the downlink,  $\theta_{rs}$  is a constant parameter that is determined by the AGC in the turn-around ranging channel.  $\theta_{rs}$  is the rms phase deviation of the downlink carrier by the ranging signal in a strong-signal scenario. In such a scenario, the noise in the transponder's ranging channel is negligible compared with the ranging signal and there is no command. This scenario occurs in a test facility before flight and in the early phase of flight when the ranging signal-to-noise ratio in the transponder's ranging channel is large. For a sinewave range clock,  $\theta_{rs}$  is related to the peak modulation index (strong signal) by:

$$\theta_{rs} = (\text{strong-signal peak modulation index for downlink ranging, rad})/\sqrt{2} \quad (17)$$

When PN ranging is done with a turn-around (non-regenerative) ranging channel, the variables  $\theta_r$ ,  $\theta_{cmd}$  and  $\theta_n$  become important. Within a turn-around channel the uplink carrier is demodulated, and the baseband signal plus noise that is the result of this demodulation is presented to a filter. The filter output is applied to an automatic gain control (AGC) circuit. The signal plus noise that exits the turn-around ranging channel is phase-modulated onto the downlink carrier.

For an arbitrary signal-to-noise ratio in a turn-around ranging channel, the rms phase deviation by ranging signal on the downlink, denoted  $\theta_r$ , is less than or equal to  $\theta_{rs}$ . Thus,  $\theta_r$  is a variable, depending on both the parameter  $\theta_{rs}$  and the ranging signal-to-noise ratio in the ranging channel.  $\theta_{rs}$  is the limiting value of  $\theta_r$ , corresponding to the strong-signal case. If

command is present on the uplink and that command passes through the transponder's ranging channel, then  $\theta_r$  also depends on the command signal-to-noise ratio in the ranging channel.

Uplink noise passes through the ranging channel and is phase-modulated onto the downlink carrier.  $\theta_n$  is the rms phase deviation by this ranging-channel noise.  $\theta_n$ , like  $\theta_r$ , is a variable that depends on both the parameter  $\theta_{r_s}$  and the ranging signal-to-noise ratio (and, possibly, also the command signal-to-noise ratio) in the ranging channel.

$\theta_{tlm}$  is the rms phase deviation of the downlink carrier due to telemetry. When the telemetry signal is bi-polar, the rms phase deviation and the peak modulation index for telemetry are identical. When a sinewave subcarrier is used with telemetry,  $\theta_{tlm}$  is related to the peak modulation index for telemetry by:

$$\theta_{tlm} = (\text{peak modulation index for telemetry, rad})/\sqrt{2}, \quad \begin{array}{l} \text{sinewave} \\ \text{subcarrier} \end{array} \quad (18)$$

### 2.3.1 Uplink

The equations of this subsection represent the case where a ranging signal and a command signal are simultaneously present on the uplink carrier. The range clock is taken here to be a sinewave. The ratio of  $P_C$  to  $P_T$ , the carrier suppression, is

$$\left. \frac{P_C}{P_T} \right|_{U/L} = J_0^2(\sqrt{2} \phi_r) \cdot S_{cmd}(\phi_{cmd}) \quad (19)$$

The ratio of  $P_R$  to  $P_T$  is

$$\left. \frac{P_R}{P_T} \right|_{U/L} = 2J_1^2(\sqrt{2} \phi_r) \cdot S_{cmd}(\phi_{cmd}) \quad (20)$$

The ratio of the fundamental command sideband power to  $P_T$  is

$$\left. \frac{P_D}{P_T} \right|_{U/L} = J_0^2(\sqrt{2} \phi_r) \cdot M_{cmd}(\phi_{cmd}) \quad (21)$$

where  $J_0(\cdot)$  and  $J_1(\cdot)$  are Bessel functions of the first kind of order 0 and 1, respectively. These functions are plotted in Figure 3. When the argument  $x$  of  $J_0(x)$  and  $J_1(x)$  is small and positive, the following approximations may be used:

$$J_0(x) \cong 1, \quad 0 \leq x \ll 1 \quad (22)$$

$$J_1(x) \cong x/2, \quad 0 \leq x \ll 1 \quad (23)$$

The suppression factor  $S_{cmd}(\phi_{cmd})$  in Equations (19) and (20) and the modulation factor  $M_{cmd}(\phi_{cmd})$  in Equation (21) depend on whether the command signal is bi-polar or uses a sinewave subcarrier. These two factors are given by:

$$S_{cmd}(\phi_{cmd}) = \begin{cases} \cos^2(\phi_{cmd}), & \text{bi-polar} \\ J_0^2(\sqrt{2} \phi_{cmd}), & \text{sinewave subcarrier} \end{cases} \quad (24)$$

$$M_{cmd}(\phi_{cmd}) = \begin{cases} \sin^2(\phi_{cmd}), & \text{bi-polar} \\ 2J_1^2(\sqrt{2} \phi_{cmd}), & \text{sinewave subcarrier} \end{cases} \quad (25)$$

In the event that command is absent from the uplink, the factor  $S_{cmd}(\phi_{cmd})$  in Equations (19) and (20) can be omitted, since  $S_{cmd}(0) = 1$ .

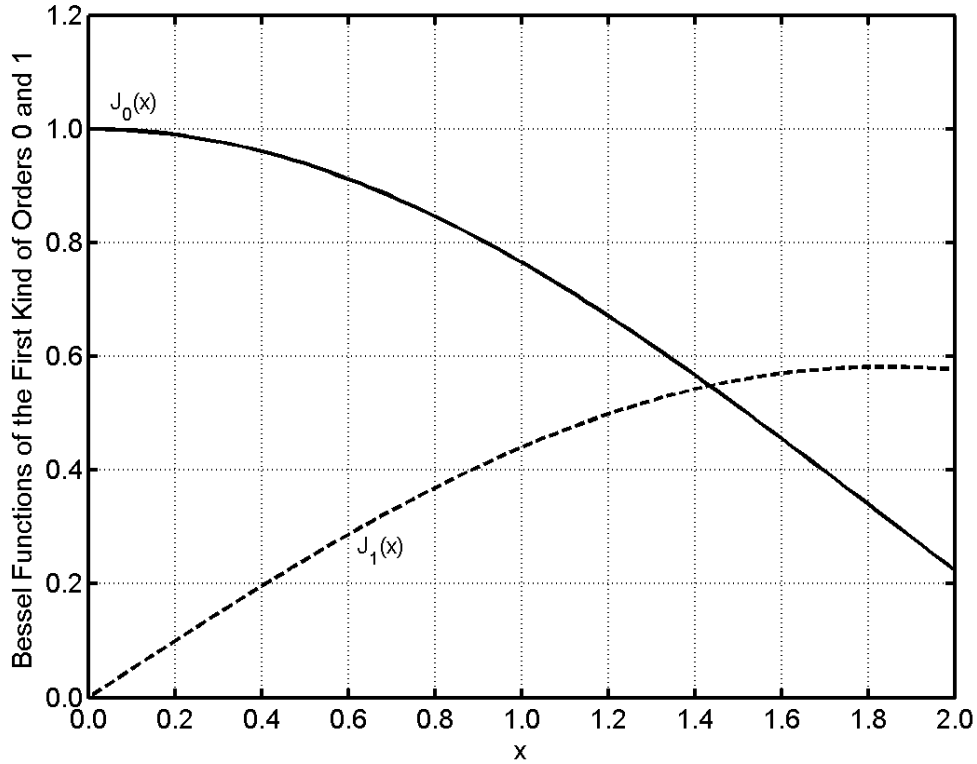


Figure 3. Bessel Functions of the First Kind of Order 0 and 1

### 2.3.2 Downlink

The equations for power allocation on the downlink depend on whether the transponder has a turn-around (non-regenerative) ranging channel or a regenerative ranging channel.

#### 2.3.2.1 Turn-Around (Non-Regenerative) Ranging

A turn-around ranging channel demodulates the uplink carrier, filters the baseband signal, applies automatic gain control, and then re-modulates the baseband signal onto the downlink carrier. The AGC serves the important purpose of ensuring that the downlink

carrier suppression is approximately constant, independent of received uplink signal level. The bandwidth  $B_R$  of the transponder's ranging channel must be larger (typically about 50% larger) than the range-clock frequency, in order to pass the ranging signal with minimal distortion. For example,  $B_R$  is typically about 1.5 MHz when the transponder is intended to accommodate a range clock of 1 MHz. Substantial thermal noise from the uplink also passes through this channel. In many deep space scenarios, the thermal noise dominates over the ranging signal in this wideband, turn-around channel. Moreover, command signal from the uplink may pass through this ranging channel. In general, then, noise and command signal as well as the desired ranging signal are modulated onto the downlink carrier whenever the ranging channel is active (Reference 3).

The equations of this subsection represent the case where a ranging signal, a (feedthrough) command signal and noise are simultaneously present in the ranging channel, so that all three of these components, plus telemetry, phase-modulate the downlink carrier. The range clock is taken here to be a sinewave. The ratio of  $P_C$  to  $P_T$ , the carrier suppression, is

$$\left. \frac{P_C}{P_T} \right|_{D/L} = J_0^2(\sqrt{2} \theta_r) \cdot S_{fth}(\theta_{cmd}) \cdot e^{-\theta_n^2} \cdot S_{tlm}(\theta_{tlm}) \quad (26)$$

The ratio of  $P_R$  to  $P_T$  is

$$\left. \frac{P_R}{P_T} \right|_{D/L} = 2J_1^2(\sqrt{2} \theta_r) \cdot S_{fth}(\theta_{cmd}) \cdot e^{-\theta_n^2} \cdot S_{tlm}(\theta_{tlm}) \quad (27)$$

The ratio of the telemetry sideband power to  $P_T$  is

$$\left. \frac{P_D}{P_T} \right|_{D/L} = J_0^2(\sqrt{2} \theta_r) \cdot S_{fth}(\theta_{cmd}) \cdot e^{-\theta_n^2} \cdot M_{tlm}(\theta_{tlm}) \quad (28)$$

where  $J_0(\cdot)$  and  $J_1(\cdot)$  are Bessel functions of the first kind of order 0 and 1, respectively.

The command-feedthrough suppression factor  $S_{fth}(\theta_{cmd})$  that appears in each of Equations (26), (27) and (28) depends on whether the command signal is bi-polar or uses a sinewave subcarrier. This factor is given by:

$$S_{fth}(\theta_{cmd}) = \begin{cases} \cos^2(\theta_{cmd}), & \text{bi-polar} \\ J_0^2(\sqrt{2} \theta_{cmd}), & \text{sinewave subcarrier} \end{cases} \quad (29)$$

In the event that command feedthrough is absent from the ranging channel, the factor  $S_{fth}(\theta_{cmd})$  in each of Equations (26), (27) and (28) can be omitted, since  $S_{fth}(0) = 1$ .

The suppression factor  $S_{tlm}(\phi_{tlm})$  in Equations (26) and (27) and the modulation factor  $M_{tlm}(\phi_{tlm})$  in Equation (28) depend on whether the telemetry signal is bi-polar or uses a sinewave subcarrier. These two factors are given by:

$$S_{tlm}(\theta_{tlm}) = \begin{cases} \cos^2(\theta_{tlm}), & \text{bi-polar} \\ J_0^2(\sqrt{2} \theta_{tlm}), & \text{sinewave subcarrier} \end{cases} \quad (30)$$

$$M_{tlm}(\theta_{tlm}) = \begin{cases} \sin^2(\theta_{tlm}), & \text{bi-polar} \\ 2J_1^2(\sqrt{2} \theta_{tlm}), & \text{sinewave subcarrier} \end{cases} \quad (31)$$

For a turn-around ranging channel, the downlink rms phase deviations  $\theta_r$ ,  $\theta_n$ , and (if command feedthrough is present)  $\theta_{cmd}$  depend on the ranging signal-to-noise ratio  $\rho_r$  and (if command feedthrough is present) the command signal-to-noise ratio  $\rho_{cmd}$  in the ranging channel.

$$\rho_r = \frac{P_R}{P_T}|_{U/L} \cdot \frac{P_T}{N_0}|_{U/L} \cdot \frac{1}{B_R} \quad (32)$$

$$\rho_{cmd} = \frac{P_D}{P_T}|_{U/L} \cdot \frac{P_T}{N_0}|_{U/L} \cdot \frac{1}{B_R} \quad (33)$$

where

$P_T/N_0|_{U/L}$  = uplink total power to noise spectral density ratio, Hz

$B_R$  = noise-equivalent (one-sided) bandwidth of transponder's ranging channel, Hz

In some transponders with a turn-around ranging channel, the AGC is designed to keep constant the average of the absolute value of the voltage at the AGC output. In other transponders, the AGC is designed to keep constant the rms voltage at the AGC output. For both types of AGC, the downlink rms phase deviations  $\theta_r$ ,  $\theta_n$ , and  $\theta_{cmd}$  depend on  $\rho_r$  and  $\rho_{cmd}$  (as well as the parameter  $\theta_{rs}$ ). Turn-around ranging channels with both types of AGC are treated below.

### 2.3.2.1.1 *AGC with Constant Average of Absolute Value of Voltage*

When the transponder's ranging channel has an AGC that keeps constant the average of the absolute value of the channel voltage, there are no exact, analytical expressions for the rms phase deviations  $\theta_r$ ,  $\theta_{cmd}$  and  $\theta_n$ . However, these rms phase deviations may be obtained by computer simulation. Curve fits to the simulations appear below.

$$\theta_r = \frac{\theta_{rs}}{1 + \exp[\gamma - 0.79 \cdot \ln(\rho_r)]} \quad (34)$$

where

$$\gamma = \begin{cases} -1.2, & \rho_{cmd} = 0 \\ \ln[0.3 + 0.27 \cdot \rho_{cmd}^{0.88}], & \rho_{cmd} > 0 \end{cases} \quad (35)$$

Here  $\exp(\cdot)$  and  $\ln(\cdot)$  are the exponential function and natural logarithm, respectively. In the event that there is no command feedthrough,  $\rho_{cmd} = 0$  and  $\theta_r$  depends only on the constant parameter  $\theta_{rs}$  and the ranging signal-to-noise ratio  $\rho_r$ . The asymptotes for Equation (34) are  $\lim_{\rho_r \rightarrow 0} \theta_r = 0$  and  $\lim_{\rho_r \rightarrow \infty} \theta_r = \theta_{rs}$ .

A similar set of equations are valid (approximately) for  $\theta_{cmd}$

$$\theta_{cmd} = \frac{\theta_{rs}}{1 + \exp[\chi - 0.79 \cdot \ln(\rho_{cmd})]} \quad (36)$$

where

$$\chi = \ln[0.3 + 0.27 \cdot \rho_r^{0.88}] \quad (37)$$

The asymptotes for Equation (36) are  $\lim_{\rho_{cmd} \rightarrow 0} \theta_{cmd} = 0$  and  $\lim_{\rho_{cmd} \rightarrow \infty} \theta_{cmd} = \theta_{rs}$ .

A curve-fit to the simulation data for  $\theta_n$  as a function of  $\rho_r$  and  $\rho_{cmd}$  is:

$$\theta_n = \frac{\theta_{rs} \cdot (2/\sqrt{\pi})}{1 + \exp[-0.87 + 0.81 \cdot \ln(\rho_{rSS})]} \quad (38)$$

where  $\rho_{rSS}$  is the root-sum-square of  $\rho_r$  and  $\rho_{cmd}$ :

$$\rho_{rSS} = \sqrt{\rho_r^2 + \rho_{cmd}^2} \quad (39)$$

The asymptotes for this curve are  $\lim_{\rho_{rSS} \rightarrow 0} \theta_n = \theta_{rs} \cdot (2/\sqrt{\pi})$  and  $\lim_{\rho_{rSS} \rightarrow \infty} \theta_n = 0$ .

Since  $\theta_r$  is directly proportional to the parameter  $\theta_{rs}$ , the ratio  $\theta_r/\theta_{rs}$  may be plotted as a function of  $\rho_r$  (and  $\rho_r$  alone when  $\rho_{cmd} = 0$ ). This appears in Figure 4 for the case of no command feedthrough:  $\rho_{cmd} = 0$  and  $\theta_{cmd} = 0$ . The solid curve labeled AAV is valid for a turn-around ranging channel whose AGC keeps constant the average of the absolute voltage (AAV). Figure 4 shows that the ratio  $\theta_r/\theta_{rs}$  increases monotonically as a function of  $\rho_r$  with a limiting value of 1. (In other words, the strong-signal value of  $\theta_r$  is  $\theta_{rs}$ .) The AAV curve of Figure 4 comes from Equations (34) and (35) with  $\rho_{cmd} = 0$ .

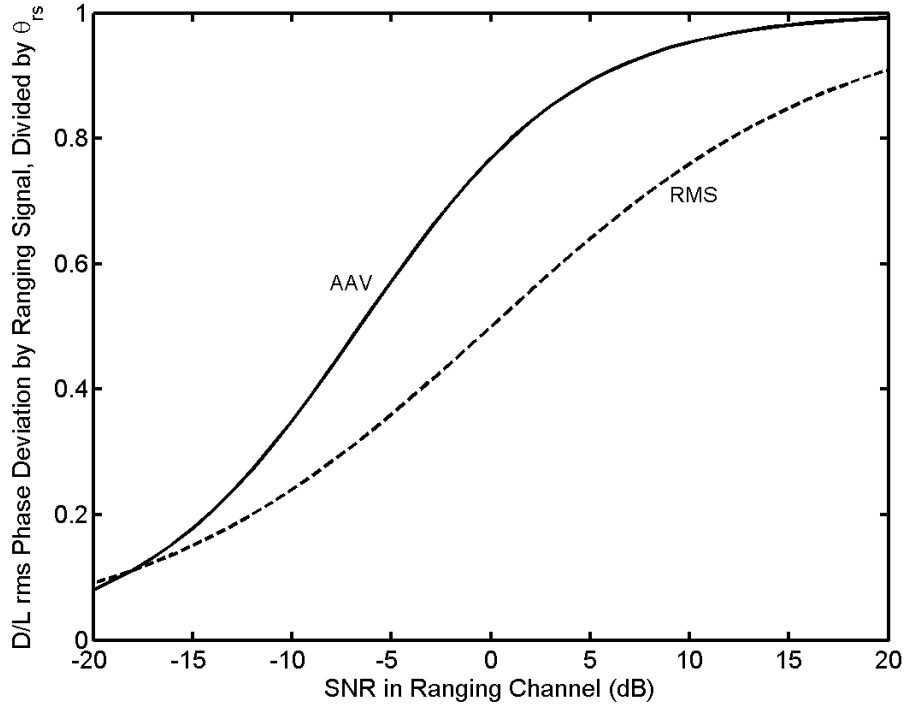


Figure 4. Downlink rms Phase Deviation by Ranging Signal (No Command Feedthrough)

The ratio  $\theta_n/\theta_{rs}$  may also be plotted as a function of  $\rho_r$  when  $\rho_{cmd} = 0$ . This appears in Figure 5. The solid curve labeled AAV is valid for a turn-around ranging channel whose AGC keeps constant the average of the absolute voltage (AAV). Figure 5 shows that the ratio  $\theta_n/\theta_{rs}$  decreases monotonically as a function of  $\rho_r$ . The AAV curve of Figure 5 comes from Equations (38) and (39) with  $\rho_{cmd} = 0$ .

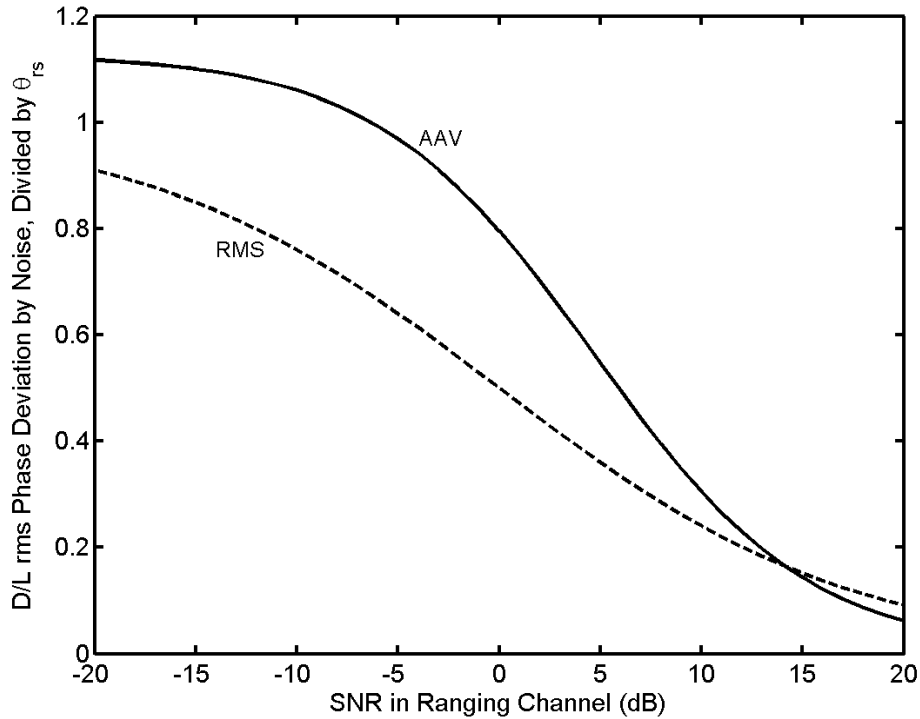


Figure 5. Downlink rms Phase Deviation by Noise (No Command Feedthrough)

### 2.3.2.1.2 AGC with Constant Root-Mean-Square Voltage

In some transponders, especially older designs, the ranging channel has an AGC that enforces a constant rms voltage at the AGC output. Since an unchanging rms voltage corresponds to an unchanging power, this type of AGC is also called a power-controlled AGC.

An AGC that enforces constant rms voltage (equivalently, constant power) at the AGC output is characterized by the following relationship among the rms phase deviations  $\theta_r$ ,  $\theta_{cmd}$ ,  $\theta_n$ , and  $\theta_{rs}$ .

$$\theta_r^2 + \theta_{cmd}^2 + \theta_n^2 = \theta_{rs}^2 \quad (40)$$

In other words, the total power in the turn-around ranging channel, which equals the ranging signal power plus the feedthrough command signal power plus the noise power in the channel bandwidth, equals a constant value. The rms phase deviations are given by

$$\theta_r = \theta_{rs} \cdot \sqrt{\frac{\rho_r}{1 + \rho_r + \rho_{cmd}}} \quad (41)$$

$$\theta_{cmd} = \theta_{rs} \cdot \sqrt{\frac{\rho_{cmd}}{1 + \rho_r + \rho_{cmd}}} \quad (42)$$

$$\theta_n = \frac{\theta_{rs}}{\sqrt{1 + \rho_r + \rho_{cmd}}} \quad (43)$$

The ratio  $\theta_r/\theta_{rs}$  is plotted as a function of  $\rho_r$  in Figure 4 for the case of no command feedthrough:  $\rho_{cmd} = 0$  and  $\theta_{cmd} = 0$ . The dashed curve labeled RMS is valid for a turn-around ranging channel whose AGC enforces a constant rms voltage at the AGC output. The RMS curve of Figure 4 comes from Equation (41) with  $\rho_{cmd} = 0$ .

The ratio  $\theta_n/\theta_{rs}$  is plotted as a function of  $\rho_r$  in Figure 5 for the case of no command feedthrough:  $\rho_{cmd} = 0$  and  $\theta_{cmd} = 0$ . The dashed curve labeled RMS is valid for a turn-around ranging channel whose AGC enforces a constant rms voltage at the AGC output. The RMS curve of Figure 5 comes from Equation (43) with  $\rho_{cmd} = 0$ .

### 2.3.2.1.3 Comparison of Two AGC Types

As explained above, there are two types of AGC that have been employed in transponders with turn-around ranging channels. These two AGCs differ in the quantity that is kept constant: either the average of the absolute voltage (AAV) or the root-mean-square (RMS).

Figure 6 plots  $P_R/P_T|_{D/L}$  as a function of  $\rho_r$  for each of the two AGC types. For all curves in this figure, there is no telemetry and there is no command feedthrough. For each AGC type, there are two curves: one for  $\theta_{rs} = 0.2$  rad rms and a second for  $\theta_{rs} = 0.4$  rad rms.  $P_R/P_T|_{D/L}$  was calculated using Equation (27). The phase deviations  $\theta_r$  and  $\theta_n$  needed within Equation (27) were calculated using the equations of Subsection 2.3.2.1.1 for the AAV curves and Subsection 2.3.2.1.2 for the RMS curves.

Figure 7 plots the carrier suppression  $P_C/P_T|_{D/L}$  as a function of  $\rho_r$  for each of the two AGC types. For all curves in this figure, there is no telemetry and there is no command feedthrough. For each AGC type, there are two curves: one for  $\theta_{rs} = 0.2$  rad rms and a second for  $\theta_{rs} = 0.4$  rad rms.  $P_C/P_T|_{D/L}$  was calculated using Equation (26). The phase deviations  $\theta_r$  and  $\theta_n$  needed within Equation (26) were calculated using the equations of Subsection 2.3.2.1.1 for the AAV curves and Subsection 2.3.2.1.2 for the RMS curves.

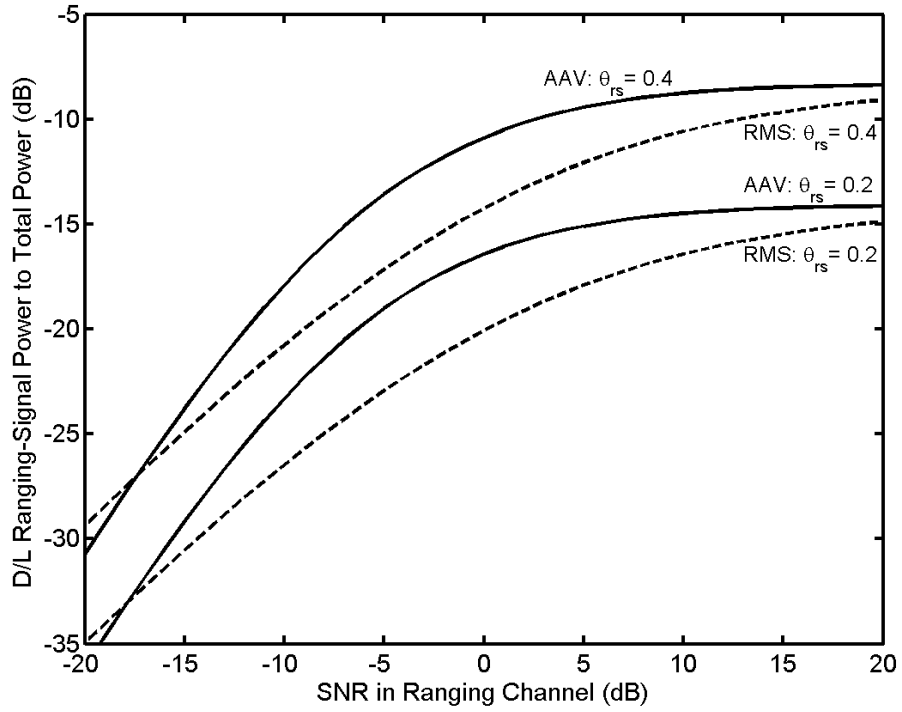


Figure 6. Downlink Ranging-Signal Power to Total Power (No Telemetry, No Command)

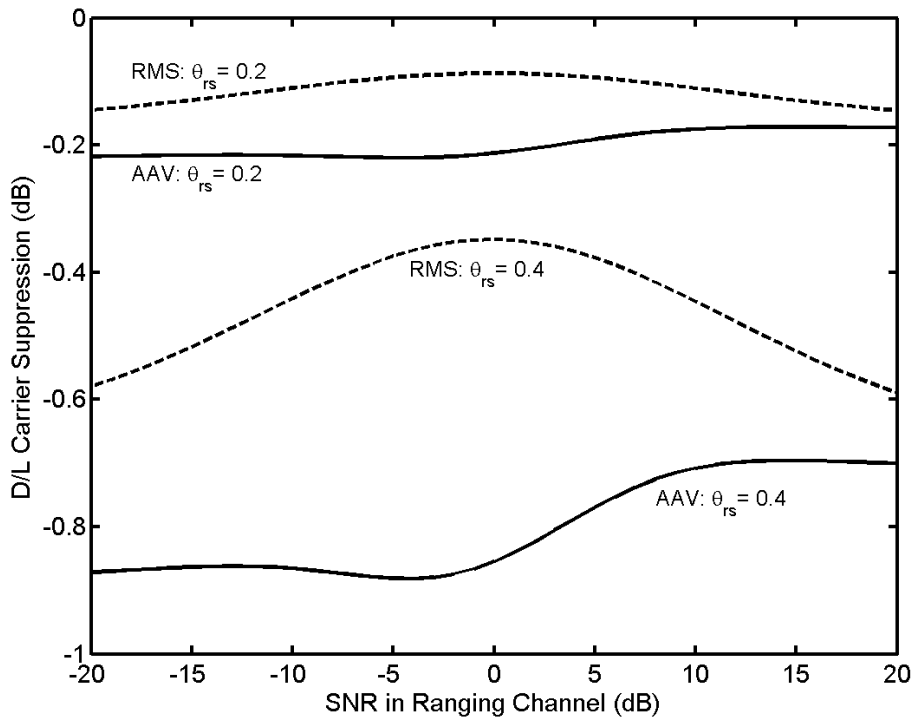


Figure 7. Downlink Carrier Suppression (No Telemetry, No Command)

### 2.3.2.2 *Regenerative Ranging*

A regenerative ranging channel demodulates the uplink carrier, tracks the range clock, detects the range code, and modulates a ranging signal on the downlink. A regenerative ranging channel produces a clean ranging signal, free of command feedthrough and with little noise, because this channel has a small bandwidth. (This bandwidth is orders-of-magnitude smaller than the 1.5-MHz bandwidth of the typical turn-around ranging channel.) For the purpose of calculating the distribution of power on the downlink in the case of regenerative ranging, the following equations may be used. There will, in general, be phase jitter on the downlink ranging signal that is caused by uplink thermal noise and this jitter is an error source for the two-way range measurement. This error is considered in Section 2.5.

The carrier suppression is

$$\left. \frac{P_C}{P_T} \right|_{D/L} = J_0^2(\sqrt{2} \theta_{rs}) \cdot \cos^2(\theta_{tlm}) \quad (44)$$

The ratio of available ranging signal power to total power is

$$\left. \frac{P_R}{P_T} \right|_{D/L} = 2 J_1^2(\sqrt{2} \theta_{rs}) \cdot \cos^2(\theta_{tlm}) \quad (45)$$

The ratio of available telemetry (data) signal power to total power is

$$\left. \frac{P_D}{P_T} \right|_{D/L} = J_0^2(\sqrt{2} \theta_{rs}) \cdot \sin^2(\theta_{tlm}) \quad (46)$$

In these equations,  $\theta_{rs}$  is the (strong-signal) rms phase deviation of the downlink carrier by the ranging signal, and  $\theta_{tlm}$  is the telemetry modulation index.

## 2.4 *Uplink Spectrum*

The spectrum of the uplink carrier is of some concern because of the very large transmitter powers used on the uplink for deep space missions. A mathematical model for this spectrum is given here for the case of a sinewave range clock and no command.

A PN ranging signal is periodic, so its spectrum consists of discrete spectral lines. The spectrum of an uplink carrier that has been phase modulated by only a PN ranging signal also consists of discrete spectral lines.

As described in Section 2.2, the composite chip sequence  $c'(\cdot)$  is similar to the range clock  $c_1'(\cdot)$ , except that some chips are inverted. A discrepancy signal  $d'(\cdot)$  is defined by

$$d'(i) = c_1'(i) \cdot c'(i) \quad (47)$$

$d'(i)$  equals +1 when the range clock and the composite code agree, which is most of the time. When the range clock and the composite code disagree,  $d'(i)$  equals -1. The PN ranging signal may be mathematically modeled as  $d(i)\sin(\pi t/T_c)$  for  $iT_c \leq t < (i+1)T_c$ , where  $T_c$  is the chip period. In words, the PN ranging signal is a sinewave (range clock) of frequency  $1/(2T_c)$  except that there is an occasional inversion of a half-cycle. When this signal phase modulates the uplink

carrier with an rms phase deviation  $\phi_r$  (radians rms), the fractional power in each discrete spectral line is given by

$$\frac{P_k}{P_T} = |X_k|^2 = \begin{cases} \text{fraction of uplink total power in the} \\ \text{discrete spectral line with frequency} \\ f_c + \frac{k}{LT_c} \end{cases} \quad (48)$$

where  $P_T$  is the total uplink power,  $f_c$  is the uplink carrier frequency,  $L$  is the period in chips of the composite code,  $k$  is an integer harmonic number, and  $X_k$  is given by

$$X_k = \frac{1}{L} \sum_{m=-\infty}^{\infty} \text{sinc}\left(\frac{m}{2} - \frac{k}{L}\right) \sum_{n=0}^{L-1} J_m(\sqrt{2} \phi_r d'(n)) \exp\left[j\pi\left(n + \frac{1}{2}\right)\left(m - \frac{2k}{L}\right)\right] \quad (49)$$

where  $J_m(\cdot)$  is the Bessel function of the first kind of order  $m$ , and

$$\text{sinc}(x) = \frac{\sin(\pi x)}{\pi x} \quad (50)$$

Equation (49) may be evaluated numerically. The values of the Bessel functions decrease very rapidly with increasing  $|m|$ , so in practice it is possible to get good accuracy while including only a few terms from the sum over the integer  $m$ . In evaluating Equation (49), the following identity is useful.

$$J_{-m}(x) = \begin{cases} J_m(x), & m \text{ even} \\ -J_m(x), & m \text{ odd} \end{cases} \quad (51)$$

There is a symmetrical power distribution about the carrier. So for every discrete spectral line at  $f_c + k/(LT)$  whose power is given by Equation (48), there is also a discrete spectral line at  $f_c - k/(LT)$  with the same power.

Figure 8 illustrates the uplink spectrum for a sinewave range clock with the DSN range code and an rms phase deviation  $\phi_r = 0.2$  rad rms. The horizontal axis represents the ratio of the frequency offset from the residual carrier to the range-clock frequency. The vertical axis is the ratio of the power in a discrete-spectral line to the total signal power, expressed in decibels. The residual carrier is located at the horizontal coordinate 0, and it has a power of  $-0.2$  dB relative to  $P_T$ . In other words, the carrier suppression is  $-0.2$  dB. The lower fundamental harmonic has a horizontal coordinate of  $-1$  (a frequency of  $f_c - f_{RC}$ ), and the upper fundamental harmonic has a horizontal coordinate of  $+1$  (a frequency of  $f_c + f_{RC}$ ); each of these has a power of  $-17.5$  dB relative to  $P_T$ . The lower second harmonic has a horizontal coordinate of  $-2$  (a frequency of  $f_c - 2f_{RC}$ ), and the upper second harmonic has a horizontal coordinate of  $+2$  (a frequency of  $f_c + 2f_{RC}$ ); each of these has a power of  $-39.7$  dB relative to  $P_T$ . The smaller spectral lines that lie between  $f_c - 2f_{RC}$  and  $f_c + 2f_{RC}$  arise from the occasional inversions of half-cycles as represented by  $d'(i)$ ; this is the spectrum spreading that permits the ambiguity to be resolved.

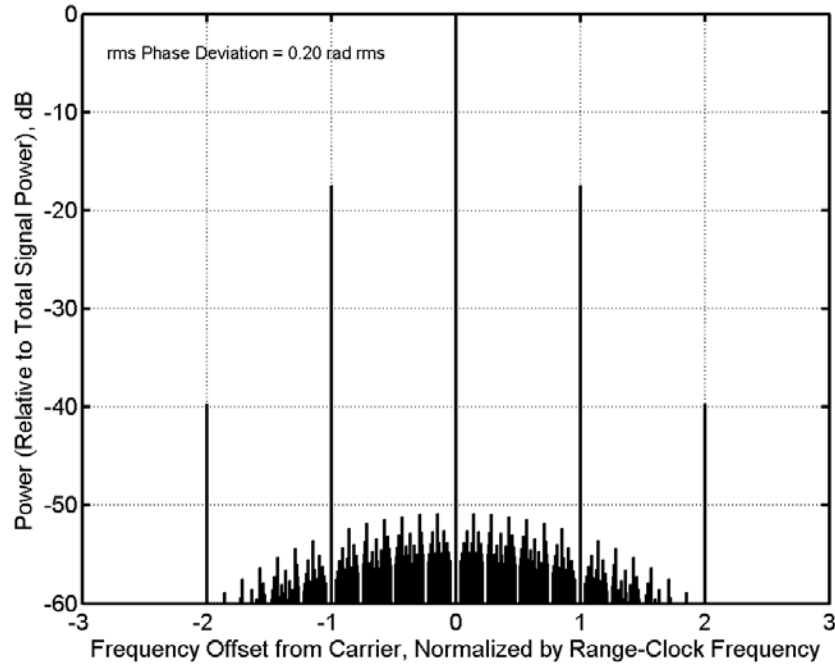


Figure 8. Uplink Spectrum for the DSN Range Code Ranging Signal

## 2.5 *Range Measurement Performance*

Thermal noise has two effects on range measurements. First, there is a standard deviation of range measurement error due to thermal noise. Second, there is a probability of acquisition of the range measurement that is less than 100% due to the presence of thermal noise. The cross-correlation factors of a composite code plays a role in the performance of PN ranging in the presence of thermal noise.

### 2.5.1 *Cross-Correlation Factors*

The cross-correlation factors  $R_n$  (with zero delay) are defined by

$$R_n = \frac{1}{L} \sum_{i=0}^{L-1} c'(i)c_n'(i) \quad (52)$$

where  $L$  is the period (in chips) of the composite code,  $c'(i) = \pm 1$  is the chip sequence, and  $c_n'(i) = \pm 1$  is the (periodic extension of the) chip sequence for the  $n$ -th component code. The cross-correlation factors are given in tables that follow: Table 3 for the DSN range code, Table 4 for the T4B code, and Table 5 for the T2B code.

Table 3. Cross-Correlation Factors, DSN Range Code

$n$	$\lambda_n$	$R_n$
1	2	0.9544
2	7	0.0456
3	11	0.0456
4	15	0.0456
5	19	0.0456
6	23	0.0456

Table 4. Cross-Correlation Factors, T4B (Reference 4)

$n$	$\lambda_n$	$R_n$
1	2	0.9387
2	7	0.0613
3	11	0.0613
4	15	0.0613
5	19	0.0613
6	23	0.0613

Table 5. Cross-Correlation Factors, T2B (Reference 4)

$n$	$\lambda_n$	$R_n$
1	2	0.6274
2	7	0.2447
3	11	0.2481
4	15	0.2490
5	19	0.2492
6	23	0.2496

### 2.5.2 *Range Measurement Error Due to Thermal Noise*

The standard deviation  $\sigma_\rho$  of range measurement error, in meters rms, due to downlink thermal noise is given by

$$\sigma_\rho = \frac{c}{f_{RC} \cdot A_c \cdot R_1 \cdot \sqrt{32\pi^2 \cdot T \cdot (P_R/N_0)}} \quad (53)$$

where

$c$  = speed of electromagnetic waves in vacuum, 299,792,458 m/s

$A_c$  = fractional loss of correlation amplitude due to frequency mismatch ( $A_c \leq 1$ )

$R_1$  = cross-correlation factor for the correlation against the range clock

$T$  = range measurement integration time

$f_{RC}$  = frequency of the range clock

$A_c = 1$  under the normal circumstances, in which the range clock is coherently related to the carrier. In the special case of non-coherent ranging,  $A_c < 1$ .

$P_R/N_0$ , the ratio of the downlink ranging signal power to the noise spectral density, is given by

$$\frac{P_R}{N_0} = \frac{P_R}{P_T} \Big|_{D/L} \cdot \frac{P_T}{N_0} \Big|_{D/L} \quad (54)$$

where  $P_T/N_0|_{D/L}$  is the downlink total signal to noise spectral density ratio and where  $P_R/P_T|_{D/L}$  is the ratio of downlink ranging signal power to total power as given by Equation (27) for turn-around (non-regenerative) ranging or as given by Equation (45) for regenerative ranging.

The factor  $P_R$  is that portion of the power in the downlink ranging sidebands that is used in the range measurement, either in the correlation that determines the range measurement error or in the resolution of the ambiguity. The power  $R_1^2 P_R$  is utilized in the correlation that determines the range measurement error. It may be noted that  $\sigma_\rho^2$ , the square of the standard deviation given in Equation (53), is inversely proportional to  $R_1^2 P_R$ . In the spectrum of the modulated downlink carrier, the power  $R_1^2 P_R$  is evenly divided between the discrete spectral line  $f_{RC}$  hertz below the residual carrier and the discrete spectral line  $f_{RC}$  hertz above the residual carrier.

For the DSN and T4B codes, the standard deviation of range measurement error (meters) due to thermal noise is plotted in Figure 9 against the product  $T \cdot (P_R/N_0)$ , expressed in decibels:  $10 \log(T \cdot P_R/N_0)$ . These curves were calculated from Equation (53) using the cross-correlation factor  $R_1$  given in Table 3 for the DSN range code and Table 4 for the T4B code. Also, the range clock was taken to be a 1-MHz sinewave and  $A_c$  was taken to be 1. The factor  $R_1$  depends on the range code. For the DSN range code,  $R_1 = 0.9544$ . For the T4B code,  $R_1 = 0.9387$ . This difference is the reason the two curves in Figure 9 do not overlap.

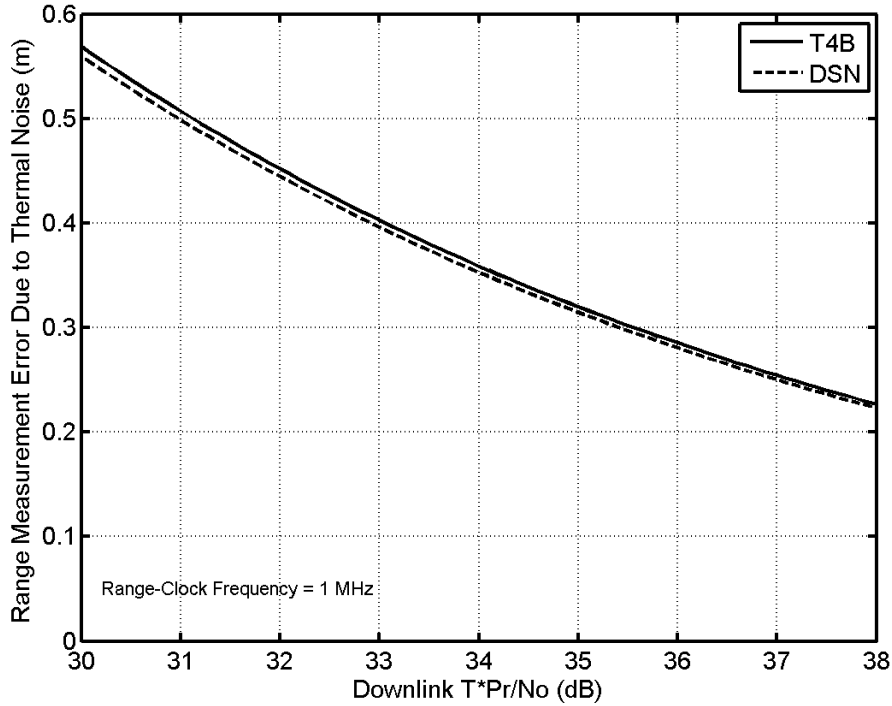


Figure 9. Standard Deviation of Range Measurement Error for the DSN and T4B Codes

The T2B code was designed to operate at smaller values of  $T \cdot (P_R/N_0)$ . For the T2B code, the standard deviation of range measurement error (meters) due to thermal noise is plotted in Figure 10. This curve was calculated from Equation (53) using the cross-correlation factor  $R_1$  given in Table 5. The range clock was taken to be a 1-MHz sinewave, and  $A_c$  was taken to be 1. The factor  $P_R$  in the product  $T \cdot (P_R/N_0)$  is that portion of the power in the downlink ranging sidebands that is used in the range measurement, either in the correlation that determines the range measurement error or in the resolution of the ambiguity.

The standard deviation of the two-way time delay  $\sigma_\tau$ , in seconds, is related to  $\sigma_\rho$ , as given in Eq. (53), by

$$\sigma_\tau = \frac{2}{c} \cdot \sigma_\rho \quad (55)$$

The factor of 2 in Eq. (55) accounts for the fact that  $\sigma_\rho$  characterizes the error in the *one*-way range, while  $\sigma_\tau$  characterizes the error in a *two*-way time delay. The standard deviation of the two-way phase delay  $\sigma_{RU}$ , as measured in range units, is related to  $\sigma_\tau$  by

$$\sigma_{RU} = \begin{cases} \frac{f_S}{2} \cdot \sigma_\tau, & \text{S-band uplink} \\ \frac{221}{749} \cdot \frac{f_X}{2} \cdot \sigma_\tau, & \text{X-band uplink} \\ \frac{221}{3599} \cdot \frac{f_{Ka}}{2} \cdot \sigma_\tau, & \text{Ka-band uplink} \end{cases} \quad (56)$$

where  $f_S$  is the frequency of an S-band uplink carrier,  $f_X$  is the frequency of an X-band uplink carrier, and  $f_{Ka}$  is the frequency of an X-band uplink carrier.

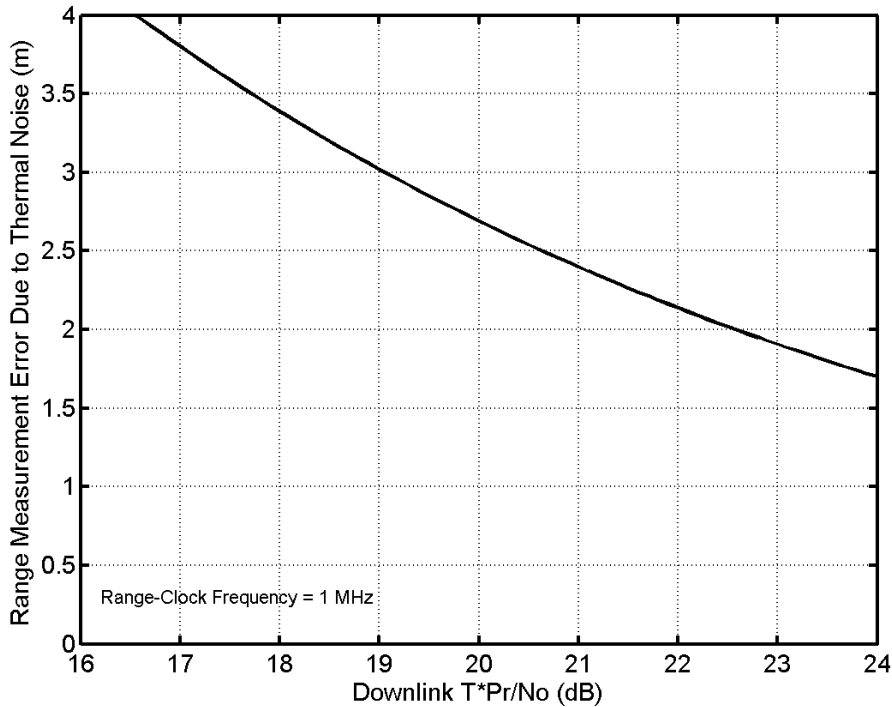


Figure 10. Standard Deviation of Range Measurement Error for the T2B Code

### 2.5.2.1 *Range Measurement Error for Turn-Around (Non-Regenerative) Ranging*

For turn-around ranging, Equation (53) accounts for both uplink and downlink thermal noise. In this case,  $P_R$  is reduced by the effect of uplink noise and any command feedthrough. This can be understood from Equation (27) by noting that  $P_R/P_T|_{D/L}$  depends on the rms phase deviations  $\theta_r$ ,  $\theta_{cmd}$ , and  $\theta_n$ .

### 2.5.2.2 *Range Measurement Error for Regenerative Ranging*

For regenerative ranging, the standard deviation  $\sigma_{RR}$  of range measurement error, in meters rms, due to uplink and downlink thermal noise is given by

$$\sigma_{RR} = \sqrt{\sigma_{\rho}^2 + \sigma_{U/L}^2} \quad (57)$$

$\sigma_{\rho}^2$  is the square of the standard deviation  $\sigma_{\rho}$  of the range measurement error due to downlink thermal noise.  $\sigma_{\rho}$  is calculated from Equation (53). In the case of regenerative ranging, this calculation uses the  $P_R/P_T|_{D/L}$  that is defined in Equation (45). This (regenerative-ranging)  $P_R/P_T|_{D/L}$  contains no contribution from uplink thermal noise.

Uplink thermal noise causes phase jitter on the regenerated ranging signal. This phase jitter arises in the tracking loop that is part of the regeneration signal processing (Reference 5). This tracking jitter is a potential error source for the two-way range measurement. The standard deviation  $\sigma_{U/L}$  of range measurement error, meters rms, for this error source is given by

$$\sigma_{U/L} = \frac{c}{4\pi R_1 f_{RC}} \sqrt{\frac{B_{RL}}{P_R/P_T|_{U/L} \cdot P_T/N_0|_{U/L}}} \quad (58)$$

where  $B_{RL}$  is the bandwidth of the loop that tracks the uplink range clock. The error  $\sigma_{U/L}$  only applies in the case of regenerative ranging. The range measurement error for a two-way, regenerative ranging measurement is computed as the root-sum-square of  $\sigma_{U/L}$  and  $\sigma_{\rho}$ , as indicated in Equation (57). For some missions it will be typical that  $\sigma_{U/L} \ll \sigma_{\rho}$ , in which case  $\sigma_{RR}$  can be approximated as  $\sigma_{\rho}$ .

Regenerative ranging has better performance than turn-around ranging. A difference in bandwidth is the reason for this. With regenerative ranging, the bandwidth of the transponder's range-clock loop,  $B_{RL}$  in Equation (58), is typically small, perhaps a few hertz. With turn-around ranging, the bandwidth  $B_R$  of the transponder's ranging channel is typically about 1.5 MHz.

### 2.5.3 *Probability of Acquisition*

A correct determination of the range can only happen if the ambiguity is correctly resolved. This is accomplished with a set of correlations within the RRT between the received baseband ranging signal and local models of the component codes. A range measurement is successfully acquired when every code component is correctly acquired. The probability of acquisition  $P_{acq}$  for the range measurement is the product of the five probabilities  $P_n$ ,  $2 \leq n \leq 6$ .

$$P_{acq} = \prod_{n=2}^6 P_n \quad (59)$$

$P_n$  is the probability of acquiring the  $n$ -th component code ( $2 \leq n \leq 6$ ). Each  $P_n$  is calculated by

$$P_n = \frac{1}{\sqrt{\pi}} \int_{-\infty}^{\infty} e^{-x^2} \left( \frac{1 + \operatorname{erf}(x + A_c R_n \sqrt{T \cdot (P_R/N_0)})}{2} \right)^{\lambda_n - 1} dx \quad (60)$$

where  $\lambda_n$  and  $R_n$  are the code length (in chips) and cross-correlation factor for the  $n$ -th component code. Numerical integration is required to evaluate Equation (60). The error function  $\text{erf}(\cdot)$  is defined by

$$\text{erf}(y) = \frac{2}{\sqrt{\pi}} \int_0^y e^{-t^2} dt \quad (61)$$

The value that Equation (59) gives for  $P_{\text{acq}}$  is, in general, greater than 0 and less than 1.  $P_{\text{acq}}$  is often characterized as a percentage (between 0% and 100%).

When interpreting Equation (60), it should be remembered that  $P_R$  is that portion of the power in the downlink ranging sidebands that is used in the range measurement. Not all of the power  $P_R$  is employed in acquisition (the resolution of the ambiguity). The power that helps with the code-component  $n$  correlation is  $R_n^2 P_R$ , where  $2 \leq n \leq 6$ .

Table 6 lists required values for  $(A_c R_n)^2 \cdot T \cdot P_R / N_0$  (in decibels) as a function of  $\lambda_n$  (the code length) and  $P_n$  (the probability of acquiring the  $n$ -th component code). This table is based on Equation (60). The first column of Table 6 is  $\log(P_n)$ , where  $\log(\cdot)$  is the common logarithm (the base-10 logarithm).

Here is an example of how Table 6 can be used. If the desired  $P_n$  for a component code of length 19 is 0.99, then  $\log(P_n) = -0.0044$ . From Table 6, the decibel values 9.9 dB and 10.1 dB are found for  $\log(P_n) = -0.005$  and  $\log(P_n) = -0.004$ , respectively. An interpolation suggests that  $(A_c R_n)^2 \cdot T \cdot P_R / N_0$  must be about 10.0 dB in order to correctly acquire with probability  $P_n = 0.99$  the component code having  $\lambda_n = 19$ . Of course, it is important to recall that  $P_n = 0.99$  is not the probability of acquisition of the composite code. There are several component codes that must be correctly acquired before the range measurement is successfully acquired.  $P_{\text{acq}}$  is given by Equation (59), and it will be less than the value of any individual  $P_n$ .

For the DSN range code and the T4B code,  $P_{\text{acq}}$  is plotted in Figure 11 as a function of the product  $T \cdot (P_R / N_0)$ , in decibels:  $10 \log(T \cdot P_R / N_0)$ . For the T2B code,  $P_{\text{acq}}$  is plotted in Figure 12 as a function of the product  $T \cdot (P_R / N_0)$ , in decibels. The curves in these two figures were calculated from Equations (59) and (60) using  $A_c = 1$  and cross-correlation factors from Table 3, Table 4, and Table 5.

Table 6. Interpolation Table

Required  $(A_c R_n)^2 \cdot T \cdot P_R / N_0$  (in decibels) for Given  $\lambda_n$  and  $P_n$

$\log(P_n)$	$\lambda_n = 7$	$\lambda_n = 11$	$\lambda_n = 15$	$\lambda_n = 19$	$\lambda_n = 23$
-0.050	5.7	6.5	6.9	7.1	7.4
-0.040	6.2	6.9	7.2	7.5	7.7
-0.030	6.7	7.3	7.7	7.9	8.1
-0.020	7.4	7.9	8.3	8.5	8.7
-0.010	8.3	8.8	9.1	9.3	9.4
-0.009	8.4	8.9	9.2	9.4	9.5
-0.008	8.6	9.0	9.3	9.5	9.7
-0.007	8.7	9.2	9.4	9.6	9.8
-0.006	8.9	9.3	9.6	9.8	9.9
-0.005	9.1	9.5	9.8	9.9	10.1
-0.004	9.3	9.7	10.0	10.1	10.3
-0.003	9.6	10.0	10.2	10.4	10.5
-0.002	9.9	10.3	10.5	10.7	10.8
-0.001	10.5	10.8	11.0	11.1	11.3

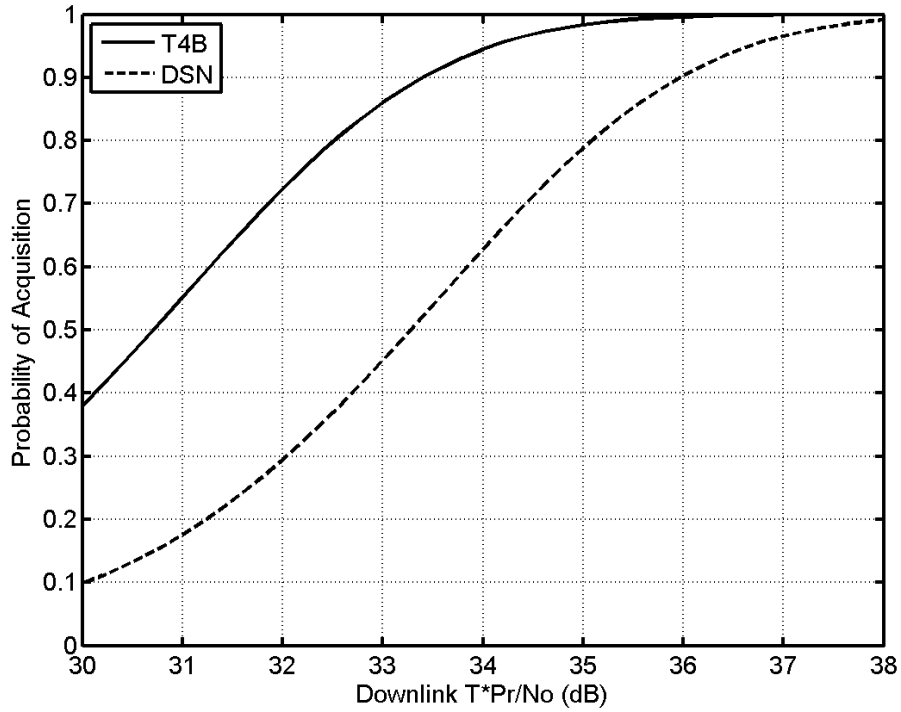


Figure 11. Probability of Acquisition for the DSN Range Code and the T4B Code

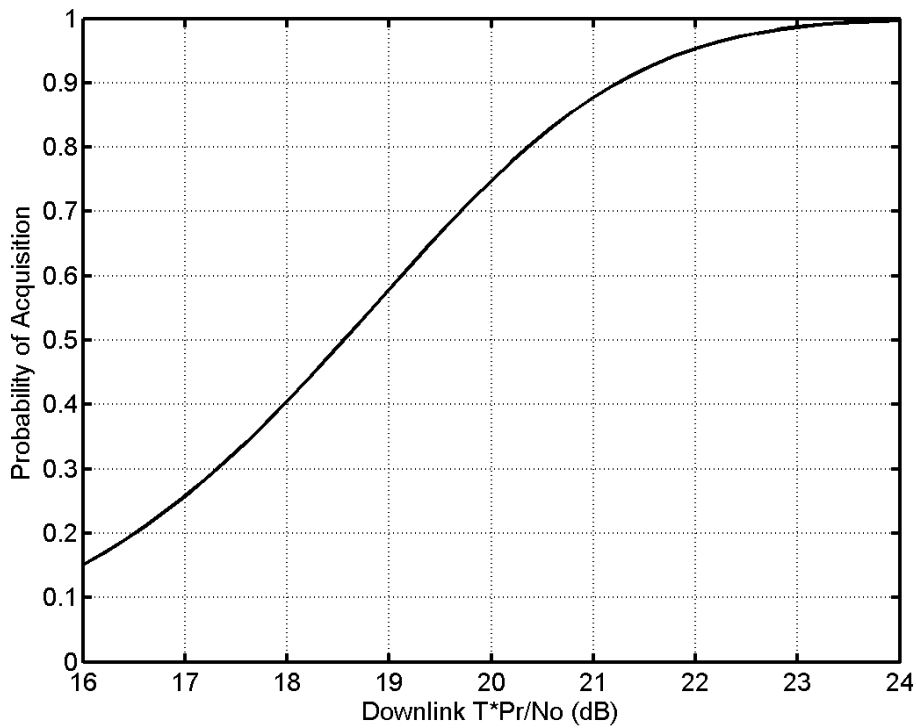


Figure 12. Probability of Acquisition for the T2B Code

An approximation of  $P_{\text{acq}}$  may be calculated using the following curve fit:

$$P_{\text{acq}} = \begin{cases} c_3 Z^3 + c_2 Z^2 + c_1 Z + c_0, & Z_1 \leq Z \leq Z_2 \\ 1.00, & Z > Z_2 \end{cases} \quad (62)$$

where  $Z$  is the product  $T \cdot (P_R/N_0)$  in units of decibels,

$$Z = 10 \log[T \cdot (P_R/N_0)] \quad \text{dB} \quad (63)$$

The parameters for the model of Equation (62) are given in Table 7. The correct set of parameters depends on the code (DSN range code, T4B, or T2B), as indicated in Table 7. The model of Equation (62) is not reliable for  $Z < Z_1$  dB. For  $Z > Z_2$  dB, the approximation  $P_{\text{acq}} = 1$  may be used.

Table 7. Parameters for Equation (62)

	DSN range code	T4B	T2B
$Z_1$	30 dB	28 dB	16 dB
$Z_2$	37 dB	35 dB	23 dB
$c_3$	-0.0039916	-0.0038441	-0.0037013
$c_2$	0.400534	0.356736	0.208431
$c_1$	-13.2253	-10.8645	-3.7427
$c_0$	144.154	109.048	21.833

Comparing Figure 9 and Figure 11, it becomes clear that the DSN range code was designed to give a  $\sigma_\rho$  of about 0.2 to 0.3 meter when the product  $T \cdot P_R/N_0$  is just large enough (about 37 to 38 dB) to assure a high probability of acquisition. The T4B code has better acquisition performance than the DSN range code. Comparing Figure 10 and Figure 12, it can be seen that the T2B code achieves a high  $P_{\text{acq}}$  for considerably smaller  $T \cdot P_R/N_0$ , but the price paid is a larger  $\sigma_\rho$ , about 2 meters.

#### 2.5.4 Processing a Set of Range Measurements

For a given PN range code, a minimum  $T \cdot (P_R/N_0)$  product is needed to achieve a high  $P_{\text{acq}}$ , and there is an approximate range measurement error (standard deviation) corresponding to this  $T \cdot (P_R/N_0)$ . In the example discussed above, the DSN range code ordinarily requires that  $T \cdot (P_R/N_0)$  be about 37 to 38 dB in order to assure a high  $P_{\text{acq}}$ , and the corresponding range measurement error is about 0.2 to 0.3 meter.

Sometimes the available  $T \cdot (P_R/N_0)$  is smaller than the minimum value for which a range code was designed to work. It is still possible to acquire range measurements with

the correct resolution of the ambiguity even under the circumstance of a low  $T \cdot (P_R/N_0)$ . This is accomplished by using a large set of range measurements (obtained from one station tracking one spacecraft).

Reference 6 describes the “Plurality Voting Method” for accomplishing range acquisitions for a large measurement data set when  $T \cdot (P_R/N_0)$  is low. This method employs range residuals for the given set of range measurements. A range residual is the difference between the measured two-way delay and the predicted two-way delay, where the predicted value is computed from a spacecraft ephemeris. Doppler velocity residuals can also be used. The Plurality Voting Method, making use of a large set of range measurements, increases the acquisition probability beyond that given in Eq. (59). This method does not, however, improve the standard deviation of acquired range measurements. The Plurality Voting Method has value in scenarios where  $T \cdot (P_R/N_0)$  is adequate for the required range accuracy (standard deviation) but is inadequate (in the absence of this special method) for the required acquisition probability.

### 2.5.5 *Comparison of PN Ranging and Sequential Ranging*

It is instructive to compare the performance of turn-around PN ranging with sequential ranging (Reference 7). For both techniques, a minimum integration time  $T$  can be calculated as a function of  $P_R/N_0$  for a given range measurement error  $\sigma_\rho$  (due to thermal noise) and a given  $P_{\text{acq}}$ . For the purpose of the present comparison,  $\sigma_\rho$  is taken to be 0.2 m and  $P_{\text{acq}}$  is taken to be 0.99. Furthermore, the range-clock frequency  $f_{RC}$  is taken to be 1 MHz.

For the analysis presented here, the minimum  $T$  is calculated for the DSN range code by finding, for a given  $P_R/N_0$ , the smallest  $T$  that satisfies the two constraints:  $\sigma_\rho < 0.2$  m, as calculated with Equation (53), and  $P_{\text{acq}} > 0.99$ , as calculated with Equations (59) and (60).

For sequential ranging, the number of sinewaves in the sequence is taken to be 20; this gives an ambiguity resolution of 78,590 km, comparable with the 75,660 km ambiguity resolution offered by the DSN range code. The minimum  $T$  for sequential ranging is the minimum cycle time consistent with a range error (due to thermal noise) of 0.2 m and a probability of acquisition of 0.99. The cycle time includes the range-clock integration time  $T_1$  plus 19 times the ambiguity integration time  $T_2$  plus the required deadtime seconds.

Figure 13 shows the ratio of the minimum  $T$  (cycle time) for sequential ranging to the minimum  $T$  (integration time) for PN ranging as a function of  $P_R/N_0$ . This figure is intended as a performance comparison of sequential ranging and turn-around PN ranging. The underlying assumption is that  $P_R/N_0$  is approximately the same for these two ranging techniques for a given set of link parameters.

In principle, a plot like this also applies to regenerative PN ranging. However,  $P_R/N_0$  will not be the same for regenerative PN ranging and (non-regenerative) sequential ranging. In general, it is expected that regenerative PN ranging will out-perform (non-regenerative) sequential ranging.

The results of Figure 13 suggest that sequential ranging has a small performance advantage over turn-around PN ranging for small  $P_R/N_0$  (less than about 12 dB-Hz for the parameters used here) but that PN ranging has a performance advantage for  $P_R/N_0$  larger than this. When the sequential ranging minimum  $T$  is larger than the PN ranging minimum  $T$  (that is,

when  $P_R/N_0$  is larger than about 12 dB-Hz), the choice to use PN ranging means that more range measurements can be made in a given period than can be made with sequential ranging.

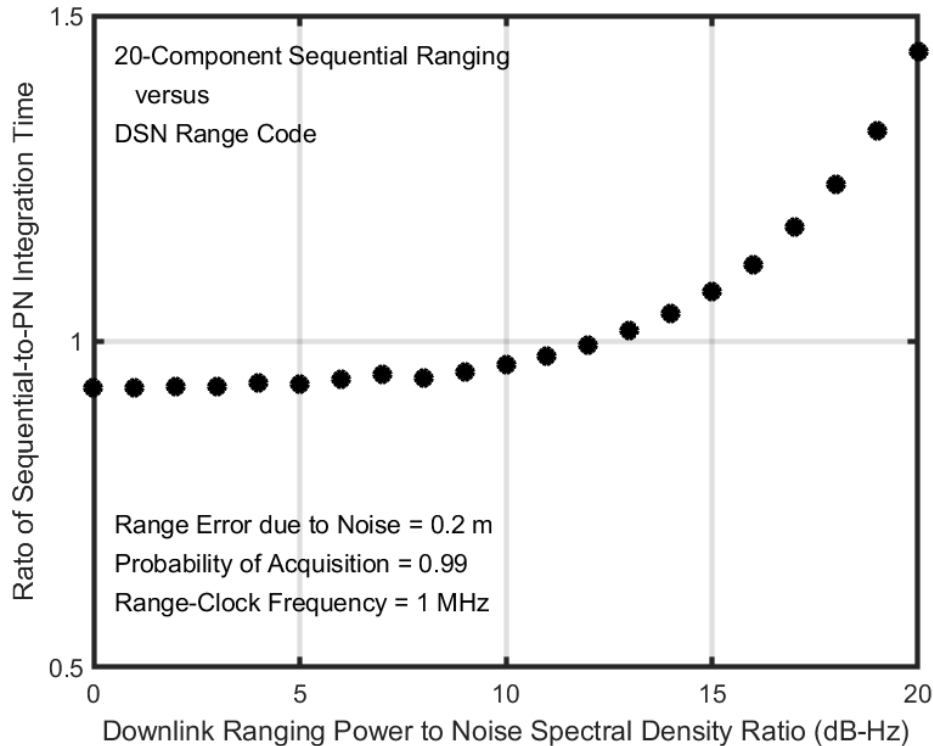


Figure 13. Comparison of Sequential Ranging and PN Ranging

PN ranging has an operational advantage over sequential ranging. With sequential ranging, a large increase in the RTL during the tracking pass forces a measurement restart. This is not an issue for PN ranging. The PN range code has a period of approximately 0.5 second when the range clock has its typical frequency of about 1 MHz. (The measurement integration time  $T$  is larger, as the measurement comprises multiple periods of the PN range code.) With PN ranging, the downlink can start processing at any 1-second boundary.

### 2.5.6 *Non-Coherent Operation*

A non-coherent ranging technique has been described in Reference 8. For the sake of economy, this technique employs a transceiver, rather than a transponder, at the spacecraft. With such a technique, the downlink carrier is not coherent with the uplink carrier, and the downlink range clock is not coherent with the downlink carrier. This means that there will ordinarily be a frequency mismatch between the received downlink range clock and its local model. This mismatch is to be minimized by Doppler compensation of the uplink carrier, but it will not be possible, in general, to eliminate completely the frequency mismatch. With this non-coherent technique, range measurement performance will not be as good as that which can be achieved with coherent operation using a transponder. Nonetheless, non-coherent range measurement performance is expected to be adequate for some mission scenarios.

The frequency mismatch inherent in non-coherent ranging has two effects on performance. One is a loss  $A_c$  of correlation amplitude, which increases the thermal noise contribution to measurement error. The other is a direct contribution to range measurement error. This direct contribution is much the more important of these two effects.

The loss of correlation amplitude is represented by  $A_c$  where  $0 < A_c < 1$ . The standard deviation  $\sigma_\rho$  of range measurement error due to thermal noise is given by Equation (53), and the probability of acquisition (considering the effect of thermal noise) is given by Equations (59) and (60). The amplitude loss factor  $A_c$  is, for non-coherent operation, given by

$$A_c = |\text{sinc}(2\Delta f_{RC}T)| \quad (64)$$

where  $\Delta f_{RC}$  is the frequency mismatch between the received range clock and its local model. The function  $\text{sinc}(\cdot)$  is defined by Equation (50). For coherent operation,  $\Delta f_{RC} = 0$  and  $A_c = 1$ .

The direct contribution of frequency mismatch to range measurement error is given by

$$\text{range error due to } \Delta f_{RC} = \frac{c}{4} \cdot \frac{\Delta f_{RC}}{f_{RC}} \cdot T, \quad \text{m} \quad (65)$$

The range error given by Eq. (65) is in meters (with  $c$  in m/s,  $T$  in seconds, and with  $\Delta f_{RC}$  and  $f_{RC}$  sharing the same units). It is worth noting that this measurement error is directly proportional to both the fractional frequency mismatch  $\Delta f_{RC}/f_{RC}$  and the measurement integration time  $T$ . The fractional frequency error will, in general, comprise two terms: a fractional frequency error due to uncertainty in the spacecraft oscillator frequency and a fractional frequency error due to imperfect uplink Doppler predicts.

Non-coherent ranging measurements should be done with regenerative ranging using PN signals. The reason for this follows. The direct error contribution due to frequency mismatch is directly proportional to the measurement integration time, as can be seen in Equation (65). So, for non-coherent operation, it is important to make  $T$  as small as possible. This is achieved with regenerative ranging, and regenerative ranging is only available with a PN ranging signal.

With non-coherent operation, the range error due to frequency mismatch increases with  $T$  and the range error due to thermal noise decreases with  $T$ . Therefore, it is important to seek an optimal value for  $T$ , in order to get the best possible performance. Reference 8 offers guidance in this matter.

## 2.6 *Range Corrections*

Range is defined to be the distance from the reference point on the DSS antenna to the reference point on the spacecraft antenna. The reference point of a DSS antenna is the intersection of the azimuth and elevation axes. When the two-way time delay is measured, the result includes more than just the two-way delay between the reference points of the DSS and spacecraft antennas. The measured two-way delay also includes station delay and spacecraft delay. These extra delays must be determined through calibration and then removed from the measured two-way time delay. The spacecraft delay is measured during DSN compatibility

testing prior to launch. The station delay is determined in two parts: the DSS delay and the Z-correction.

A range measurement (that has not yet been corrected) provides the two-way delay through the station uplink path, starting from the USG, to and from the spacecraft, and through the station downlink path, ending in the RRT. Figure 14 illustrates the two-way signal path at the station. It is necessary to determine the uplink station delay for the path from the USG to the antenna reference point, to determine the downlink station delay for the path from the antenna reference point to the RRT, and to remove these delays from the measured two-way delay.

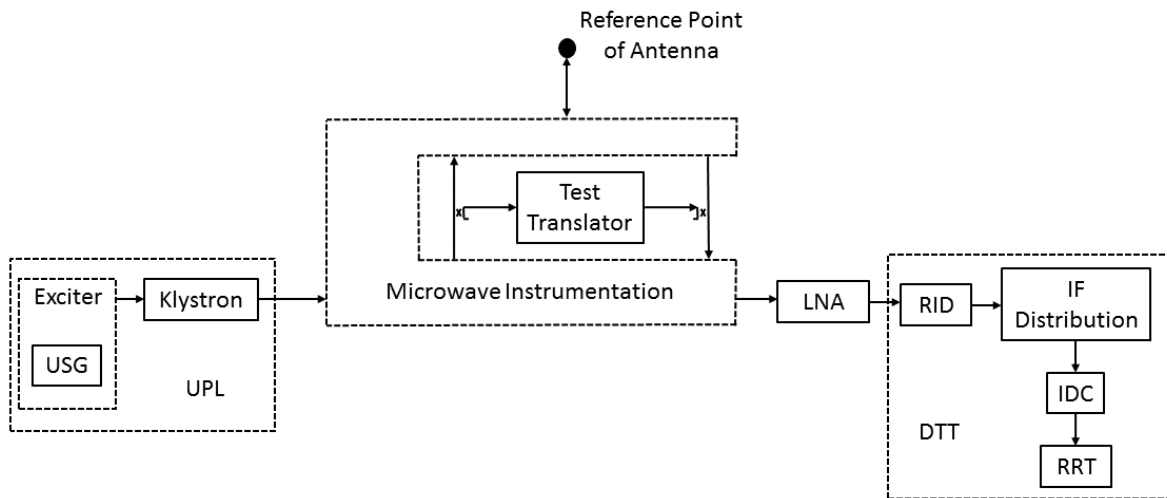


Figure 14. DSS Delay Calibration

### 2.6.1 DSS Delay

The DSS delay is obtained by a calibration that mimics an actual two-way range measurement, except that the signal path lies entirely within the station. A portion of the uplink carrier is diverted through a coupler to a test translator. The test translator shifts the carrier to the downlink frequency (while not altering the modulation) and feeds this frequency-shifted carrier to a coupler that places it on the downlink path within the station. The DSS delay contains most of the station delay. To be precise, the DSS delay comprises the delay from the USG to the ranging coupler on the uplink, the delay through the test translator (and its cables), and the delay from the ranging coupler on the downlink to the RRT.

Figure 14 is a somewhat abstract representation of the configuration. The microwave instrumentation shown in this figure is not an official subsystem, rather it is a conceptual grouping of microwave signal paths and microwave devices. On the uplink, the uplink carrier that is output from the klystron passes through the microwave instrumentation on its way to the reference point of the antenna. On the downlink, the downlink passes through the microwave instrumentation on its way to the LNA. Along the uplink path, a portion of the uplink carrier is coupled to the test translator. The portion of the carrier that has been frequency shifted to the downlink band inside the test translator is then coupled to the downlink path. The specific details of the microwave instrumentation are generally different at different DSSs and

for different bands within a given DSS. Modules 101, 103 and 104 should be consulted for those details.

The DSS delay is station and configuration dependent. It should be measured for every ranging pass. This measurement is called precal for pre-track calibration and postcal for post-track calibration. The former is done at the beginning of a ranging pass; the latter is only needed when there is a change in equipment configuration during the track or precal was not performed due to a lack of time.

The DSS delay varies significantly as a function of carrier frequency. This is illustrated in Figure 15 for an X-band (uplink and downlink) calibration at DSS 63. The vertical axis on this plot is the DSS delay, labeled STDL in this plot. The difference between the largest and smallest delays over the 8400—8450 MHz band is about 18 ns in this case. On both the lower and upper ends of this band, the rise in station delay originates in the klystron on the uplink side of the station. The ripple in the station delay arises from impedance mismatches; every transmission line that has some mismatch at both ends will introduce ripple in the group delay.

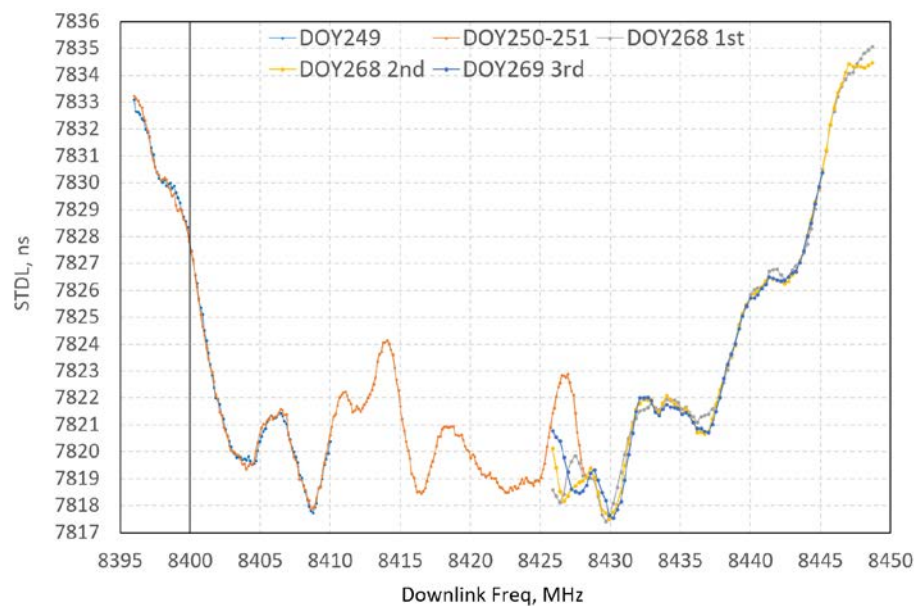


Figure 15. DSS Delay as a Function of Downlink Frequency

### 2.6.2 Z-Correction

The DSS delay itself must be corrected. This is accomplished with the Z-correction. The DSS delay includes the delay through the test translator (and its cables), but the test translator is not in the signal path of an actual range measurement. Moreover, the DSS delay does not include, but should include, the delays between the ranging couplers and the antenna reference point.

The Z-correction is defined as the delay through the test translator (and its cables) minus the uplink and downlink delays between the ranging couplers and the antenna reference point. The DSS delay minus the Z-correction therefore gives the delay between the USG and the antenna reference point plus the delay between the antenna reference point and the RRT. This is exactly the quantity that must be subtracted from a range measurement in order to produce a two-way delay relative to the antenna reference point.

The test translator delay is measured by installing a zero delay device (ZDD) in place of the test translator. Since the ZDD delay is measured in the laboratory, the signal delay contributed by the test translator can be calculated to a known precision. This measurement is made approximately once each year or when there are hardware changes in this portion of the signal path. The delays between the ranging couplers and the antenna reference point are stable and need not be updated often; they are determined by a combination of calculation and measurement.

## **2.7        *Total Error for Range Measurement***

Several error sources contribute to the total error for a range measurement. For two-way range measurement, the two most important error sources are typically thermal noise and station calibration error. The error due to thermal noise is discussed in Section 2.5. The error in calibrating and removing the station delay is often the dominant error source for two-way ranging. For two-way range measurements in the X band, there is typically about 6 ns of station calibration error in the two-way delay, corresponding to a (one-way) range error of about 1 meter.

The error in calibrating and removing the spacecraft delay is stable for a given spacecraft and a given band pairing (for example, X band on the uplink and X band on the downlink). The orbit determination program can, given enough range measurements for this spacecraft and band pairing, solve for this error.

There are error contributions, usually small compared to the station calibration error, due to the passage of the uplink and downlink through the troposphere, ionosphere and solar corona (Reference 9). When the angle between the sun and the spacecraft, as seen from the station, is small and the spacecraft is beyond the sun, the error contribution from the solar corona can become the dominant contributor to error in the range measurement.

For three-way ranging (in which one station transmits the uplink and a second station receives the downlink), the total delay measurement error is larger than for two-way. There are two reasons for this. First, there is a clock offset between the transmitting and receiving stations. Second, the calibration of the station delays is more difficult to achieve accurately in this case.

## ***Appendix: Glossary of Parameters***

$P_T/N_0 _{U/L}$	ratio of uplink total power to noise spectral density, Hz
$P_C/P_T _{U/L}$	ratio of uplink residual-carrier to total power
$P_R/P_T _{U/L}$	ratio of uplink ranging-signal to total power
$P_D/P_T _{U/L}$	ratio of uplink command-signal to total power
$P_T/N_0 _{D/L}$	ratio of downlink total power to noise spectral density, Hz
$P_C/P_T _{D/L}$	ratio of downlink residual-carrier to total power
$P_R/P_T _{D/L}$	ratio of downlink ranging-signal to total power
$P_D/P_T _{D/L}$	ratio of downlink telemetry to total power
$P_R/N_0$	ratio of downlink ranging-signal power to noise spectral density, Hz
$P_k/P_T$	ratio of discrete spectral line power to total power
$Z$	$T \cdot (P_R/N_0)$ in decibels
$\rho_\rho$	ranging signal-to-noise ratio in transponder's ranging channel
$\rho_{cmd}$	command-feedthrough signal-to-noise ratio in transponder's ranging channel
$B_R$	noise-equivalent bandwidth of transponder's ranging channel, Hz
$B_{RL}$	noise-equivalent bandwidth of uplink code-tracking loop, Hz
$T$	integration time for range measurement, s
$T_c$	chip period, s
$f_{chip}$	chip rate, Hz
$f_{RC}$	range-clock frequency, Hz
$f_C$	frequency of residual carrier, Hz
$f_S$	S-band carrier frequency, Hz
$f_X$	X-band carrier frequency, Hz
$f_{Ka}$	Ka-band carrier frequency, Hz
$\Delta f_{RC}$	difference between the received range-clock frequency and its local model, Hz
$A/B$	rational factor that, together with the uplink carrier frequency, sets the chip rate
$c$	speed of electromagnetic waves in vacuum, m/s

$\lambda_n$	period of $n$ -th component code
$L$	length of composite code
$R_n$	cross-correlation factor of code component $n$ against composite code
$A_c$	fractional loss of correlation amplitude due to non-coherent frequency mismatch
$\phi_r$	phase deviation of uplink carrier by ranging signal, rad rms
$\phi_{cmd}$	phase deviation of uplink carrier by command signal, rad rms
$\theta_{rs}$	phase deviation of downlink carrier by ranging signal (strong signal), rad rms
$\theta_r$	phase deviation of downlink carrier by ranging signal, rad rms
$\theta_{cmd}$	phase deviation of downlink carrier by command feedthrough, rad rms
$\theta_n$	phase deviation of downlink carrier by noise, rad rms
$\theta_{tlm}$	telemetry modulation index, rad
$S_{cmd}(\phi_{cmd})$	suppression factor on uplink due to command
$M_{cmd}(\phi_{cmd})$	modulation factor on uplink for command
$S_{fth}(\theta_{cmd})$	suppression factor on downlink due to command feedthrough
$S_{tlm}(\theta_{tlm})$	suppression factor on downlink due to telemetry
$M_{tlm}(\theta_{tlm})$	modulation factor on downlink for telemetry
$P_n$	probability of acquiring the $n$ -th component code
$P_{acq}$	probability of acquisition
$\sigma_\rho$	standard deviation of range measurement error due to downlink noise, m
$\sigma_{U/L}$	standard deviation of range measurement error due to uplink noise, m
$\sigma_{RR}$	standard deviation of range measurement error due to all noise, m
$\sigma_\tau$	standard deviation of two-way delay, s
$\sigma_{RU}$	standard deviation of the two-way phase delay, RU

## ***References***

1. J. B. Berner, S. H. Bryant, and P. W. Kinman, "Range Measurement as Practiced in the Deep Space Network," *Proceedings of the IEEE*, Vol. 95, No. 11, November 2007.
2. Consultative Committee for Space Data Systems, "Pseudo-Noise (PN) Ranging Systems," CCSDS 414.1-B-2, February 2014.
3. P. W. Kinman and J. B. Berner, "Two-Way Ranging During Early Mission Phase," *2003 IEEE Aerospace Conference*, March 8-15, 2003, Big Sky, MT.
4. J. L. Massey, G. Boscagli, and E. Vassallo, "Regenerative Pseudo-Noise (PN) Ranging Sequences for Deep-Space Missions," *Int. J. Satellite Communications and Networking*, Vol. 25, No. 3, pp. 285-304, May/June 2007.
5. J. B. Berner, J. M. Layland, P. W. Kinman, and J. R. Smith, "Regenerative Pseudo-Noise Ranging for Deep-Space Applications," *TMO Progress Report 42-137*, Jet Propulsion Laboratory, Pasadena, CA, May 15, 1999.
6. J. R. Jensen, "A Plurality Voting Method for Acquisition of Regenerative Ranging Measurements," *2013 IEEE Aerospace Conference*, March 2-9, 2013, Big Sky, MT.
7. J. B. Berner and S. H. Bryant, "Operations Comparison of Deep Space Ranging Types: Sequential Tone vs. Pseudo-Noise," *2002 IEEE Aerospace Conference*, March 9-16, 2002, Big Sky, MT.
8. M. K. Reynolds, M. J. Reinhart, R. S. Bokulic, and S. H. Bryant, "A Two-Way Noncoherent Ranging Technique for Deep Space Missions," *2002 IEEE Aerospace Conference*, March 9-16, 2002, Big Sky, MT.
9. C. L. Thornton and J. S. Border, *Radiometric Tracking Techniques for Deep-Space Navigation*, Monograph 1 of the *Deep-Space Communications and Navigation Series*, Jet Propulsion Laboratory, Pasadena, CA, 2000.